Sociosexual behavior requires both activating and repressive roles of Tfap2e/AP-2ε in vomeronasal sensory neurons

Jennifer M. Lin[1,2], Tyler A. Mitchell[1,2], Megan Rothstein[3], Alison Pehl[1,2], Ed Zandro M. Taroc[1,2], Raghu R. Katreddi[1,2], Katherine E. Parra[4], Damian G. Zuloaga[4], Marcos Simoes-Costa[3], and Paolo E. Forni[1,2,*]

[1]Department of Biological Sciences, University at Albany, Albany, NY, USA.

[2]The RNA Institute, University at Albany, Albany, NY, USA.

[3]Department of Molecular Biology and Genetics, Cornell University, Ithaca, New York 14850, USA

[4]Department of Psychology, University at Albany, Albany, NY, USA.

*Corresponding Author

SUMMARY

Neuronal identity dictates the position in an epithelium, and the ability to detect, process, and transmit specific signals to specified targets. Transcription factors (TFs) determine cellular identity via direct modulation of genetic transcription and recruiting chromatin modifiers. However, our understanding of the mechanisms that define neuronal identity and their magnitude remains a critical barrier to elucidate the etiology of congenital and neurodegenerative disorders. The rodent vomeronasal organ provides a unique system to examine in detail the molecular mechanisms underlying the differentiation and maturation of chemosensory neurons. Here we demonstrated that the identity of postmitotic/maturing VSNs and vomeronasal dependent behaviors can be reprogrammed through the rescue of AP-2ε expression in the AP-2ε^{Null} mice and by inducing ectopic AP-2ε expression in mature apical VSNs. We suggest that the transcription factor AP-2ε can reprogram VSNs bypassing cellular plasticity restrictions, and that it directly controls the expression of batteries of vomeronasal genes.

KEYWORDS

Vomeronasal, Transcription Factor, Tfap2e/AP-2ε, Neuronal Identity, Single-Cell Sequencing, scRNA-seq, CUT&RUN, Chromatin Architecture, Cellular Plasticity, behavior, basal vomeronasal sensory neurons, accessory olfactory bulb, differentiation

INTRODUCTION

Neuronal differentiation is controlled by the selective expression of transcription factors (TFs), chromatin modifiers, and other regulatory factors that reduce cellular plasticity. During neuronal differentiation terminal selectors can activate identity-specific genes that define functional properties specific to a particular neuronal type. However, reprograming postmitotic neurons by ectopically expressing terminal selectors in *C. elegans* suggests that the "reprogrammability" of neurons is progressively lost during postembryonic life (Patel and Hobert, 2017; Patel et al., 2012; Rahe and Hobert, 2019). This reduction in cellular plasticity may arise from chromatin modifications that prevent the activation of alternative differentiation programs. However, sensory neurons of the vomeronasal organ in rodents can undergo some postnatal reprogramming following the aberrant expression of transcription factors (Lin et al., 2018).

The accessory olfactory system (AOS) contains the vomeronasal organ (VNO), which is primarily responsible for detecting odors and chemosignals that trigger social and sexual behaviors (Trouillet et al., 2019; Trouillet et al., 2021). The vomeronasal sensory epithelium of rodents is mainly composed vomeronasal sensory neurons (VSN). The VSN populations selectively express only one or two receptors encoded by the two vomeronasal receptor (VR) gene families: V1R and V2R (Dulac and Axel, 1995; Herrada and Dulac, 1997; Matsunami and Buck, 1997; Ryba and Tirindelli, 1997). V1R and V2R-expressing neuronal populations each detect distinct chemosignals, induce different innate behaviors, show distinct localization patterns in the VNO, and project to specific areas of the accessory olfactory bulb (AOB) (Cloutier et al., 2002; Dulac and Axel, 1995; Isogai et al., 2011; Katreddi and Forni, 2021; Mohrhardt et al., 2018; Mombaerts et al., 1996; Stowers et al., 2002). The V2R-expressing neurons localize to the basal portions of the vomeronasal epithelium (VNE) and around the vasculature (Naik et al., 2020), while V1R-expressing neurons localize to the apical part. Basal and apical VSNs continually regenerate from common pools of Achaete Scute like-1 (Ascl-1)-positive neural progenitor cells (NPCs) localized in the lateral and basal margins of the VNE (Cau et al., 1997; de la Rosa-Prieto et al., 2010; Katreddi and Forni, 2021; Martinez-Marcos et al., 2000; Murray et al., 2003). However, we are only starting to understand how the apical and basal VSN cell differentiation programs are initiated and which factors aide in

63 maintaining apical and basal neuronal identity (Enomoto et al., 2011; Katreddi et al., 2021;
64 Lin et al., 2018; Naik et al., 2020; Oboti et al., 2015).
65 Establishing functional basal and apical VSNs is crucial for intra- and interspecies
66 social interactions in rodents. Deficits in basal neuron functionality prevented sex
67 discrimination, reduced male-male and maternal aggressive behaviors, and inhibited the
68 detection of predator odors (Chamero et al., 2011; Stowers et al., 2002).
69 Transcription factors can drive cellular processes that control the expression of
70 genes defining their cellular and functional identity. The AP-2 family of transcription
71 factors is comprised of 5 members AP-2α, AP-2β, AP-2γ, AP-2δ and AP-2ε, which are
72 encoded by distinct genes (TFAP2A, TFAP2B, TFAP2C, TFAP2D, TFAP2E) (Eckert et
73 al., 2005; Pellikainen and Kosma, 2007; Wankhade et al., 2000). AP-2 family members
74 play critical roles during development, such as contributing to neural crest differentiation
75 (Luo et al., 2020; Rothstein and Simoes-Costa, 2020), cell specification, limb
76 development, and organogenesis (Bassett et al., 2012; Chambers et al., 2019; Kantarci
77 et al., 2015). Some AP-2 family members may have pioneer factor properties (Fernandez
78 Garcia et al., 2019; Rothstein and Simoes-Costa, 2020; Seberg et al., 2017; Williams et
79 al., 2009).
80 Aside from the AP-2 family, Bcl11b and Tfap2e/AP-2ε control Gαo+ VSNs'
81 differentiation and survival (Enomoto et al., 2011). We proposed that AP-2ε, which is only
82 expressed after the apical and basal VSN dichotomy is established, is necessary for
83 further specification of basal VSN identity (Lin et al., 2018). Using mice expressing non-
84 functional AP-2ε, we discovered that VSNs can still acquire the Gαo+/basal identity;
85 however, these VSN have reduced survival and can acquire some Gαi2+/apical VSNs
86 molecular features over time (Lin et al., 2018). While we examined the role of AP-2ε in
87 maintaining cellular identity and homeostasis of the vomeronasal epithelium, critical
88 outstanding questions remain unresolved. What role does this transcription factor actively
89 play to control the basal genetic program? What is the extent of cellular plasticity in
90 differentiated neurons in mammals (Patel and Hobert, 2017; Rahe and Hobert, 2019)?
91 Here, we aimed to understand 1) if AP-2ε functions as a terminal selector factor
92 for basal VSNs, 2) how much cellular plasticity postmitotic neurons retain once
93 differentiated, and 3) to what extent genetic dysregulation in mature VSNs translates into

behavioral changes. We generated a Cre inducible mouse line, where we inserted the mTfap2e/AP-2ε gene into the ROSA26 locus. Using this knock-in mouse line, we could 1) rescue the AP-2ε KO's VNO morphology and functionality and 2) ectopically express AP-2ε in maturing Gαi2+/apical VSNs. This approached enable us to assess its ability to reprogram differentiated apical VSNs to basal VSNs. By combining histological analyses, behavioral assessments, and single-cell RNA sequencing (scRNA-seq) analysis, we examined whether AP-2ε functioned as a master regulator to reprogram differentiated neurons and alter animal behaviors. In addition, we used CUT&RUN (Skene et al., 2018) to identify direct genetic targets of AP-2ε that controls the basal VSNs identity program. Overall, we suggest that AP-2ε partially functions as a terminal selector for basal VSN neuronal identity by activating some basally enriched genes while simultaneously suppressing specific apically enriched genes.

RESULTS

Transcriptome differences between apical and basal VSNs

Using single cell RNA-sequencing (scRNA-Seq) on VNOs from OMPCre+ control mice at P10, we identified key features of VSNs based on the expression plots. We then clustered single cells into representative UMAPs (Figure 1). Ascl1(Figure 1A), Neurogenin1 (Neurog1) (Figure 1B), and NeuroD1 (Figure 1C) expression identified proliferative VSN progenitors (Katreddi and Forni, 2021). We determined that the dichotomy of apical-basal differentiation begins when the cells transition from Neurog1 to NeuroD1 expression, and during the NeuroD1 phase (Figure 1B,C)(Katreddi et al., 2021). The later stages of apical and basal VSN maturation were marked by the expression of Gap43 (Figure 1D) in immature neurons and OMP (Figure 1E) in more mature VSNs (Katreddi and Forni, 2021).

Consistent with prior reports, Bcl11b was expressed in Neurog1/NeuroD1 precursors and in differentiating apical and basal VSNs. While Bcl11b was expressed as a continuum along the basal differentiation trajectory, Bcl11b was not expressed in the apical neurons until later stages of maturation (Figure 1F, (Enomoto et al., 2011; Katreddi et al., 2021)). The transcription factor Meis2 was expressed in progenitor cells, and differentiating and maturing apical neurons, but not in differentiating basal VSNs (Figure

125 1G). In addition, Tfap2e/AP-2ε (Figure 1H) was expressed in maturing and mature basal
126 VSNs after the apical-basal differentiation dichotomy was established, in line with our
127 prior work (Lin et al., 2018). Using scRNA-Seq between mature (OMP+) apical and basal
128 VSNs, we confirmed the differential expression of known markers for either apical or basal
129 VSNs (e.g. Meis1, Meis2, Gnai2/Gαi2, and Nrp2 for apical and Gnao1/Gαo, Tfap2e/AP-
130 2ε, and Robo2 for basal). However, we also identified numerous unreported genes that
131 were significantly enriched in apical and basal VSNs ($q<0.05$, Figure 1J, Supplementary
132 Table S1). Among these, we validated Keratin18 (Krt18) as a novel marker for basal VSNs
133 using histochemistry (Figure1J, Figure2K-M).
134
135 **Inducible R26AP2ε rescues basal VSNs in AP-2ε KOs**
136 We hypothesized that Tfap2e (AP-2ε) can control gene expression during basal
137 VSN maturation. So, we generated a new Cre inducible mouse line (B6.Cg-
138 Gt(ROSA)26Sor$^{tm(CAG\text{-}mTfap2e)For}$). We inserted a lox-P-flanked stop cassette to prevent the
139 transcription of a CAG promoter driven murine Tfap2e gene, which was knocked into the
140 first intron of the Gt(ROSA)26Sor locus (Figure 2A). We refer to this as R26AP2ε. AP-2ε
141 expression is normally restricted to basal regions of the VNO with higher expression
142 levels of AP-2ε in the neurogenic marginal zones (Enomoto et al., 2011; Lin et al., 2018;
143 Naik et al., 2020)(Figure 2 B,B'). To test our Cre inducible AP-2ε line, we performed anti-
144 AP-2ε immunostaining on wild-type controls, AP-2ε$^{Cre/Cre}$ (AP-2ε^{Null})(Feng et al., 2009; Lin
145 et al., 2018), and AP-2ε$^{Cre/Cre}$ /R26AP2ε (AP-2ε^{Rescue}) mice (Figure 2B-D). As expected,
146 wild-type mice showed AP-2ε immunoreactivity in the basal regions of the VNE with
147 strong immunoreactivity in proliferative regions (Figure 2B, B'). However, in AP-2ε^{Null}
148 mice, where Cre was knocked into the DNA binding domain of AP-2ε (Feng et al., 2009;
149 Feng and Williams, 2003), we observed faint AP-2ε cytoplasmic immunoreactivity limited
150 to the most marginal zones of the VNO and no immunoreactivity in the rest of the
151 neuroepithelium (Figure 2C, C'). AP-2ε^{Rescue} mice showed restored AP-2ε
152 immunoreactivity in the basal region of the VNE. However, we observed that the AP-2ε
153 expression pattern and immunoreactivity were not identical to controls in the neurogenic
154 regions. In AP-2ε^{Rescue} mice, we observed no AP-2ε immunoreactivity at the tips of the

155 neurogenic niche in the VNE (Figure 2D'), suggesting a delayed AP-2ε expression after
156 AP-2εCre mediated recombination compared to controls (Figure 2B',D').
157 By analyzing the expression of the basal markers downregulated in AP-2ε KOs
158 (Lin et al., 2018), such as V2R2 (Figure 2E-G) and Gαo (Figure 2H-J), we confirmed
159 restored expression in the rescued KOs. Cell quantifications indicated a significant
160 increase in the number of basal cells expressing basal markers in AP-2ε^{Rescue} compared
161 to AP-2ε^{Null} mice, though the number of basal VSNs in the AP-2ε^{Rescue} was smaller when
162 compared to controls. Keratin18 (Krt18) is normally enriched in basal neurons (Figure 1J).
163 Immunohistochemistry confirmed Krt18 protein expression in the basal territories of the
164 VNO (Figure 2K). We observed reduced Krt18 immunoreactivity in AP-2ε^{Null} mice and
165 restored expression in AP-2ε^{Rescue} mice (Figure 2L-N). However, in AP-2ε^{Rescue} mice,
166 Krt18 still showed lower expression levels than in WT mice (Figure 2N). Taken together,
167 we conclude that exogenous AP-2ε in postmitotic VSNs can partially rescue the
168 expression of basal VSN markers in AP-2ε^{Nulls} mice. Rescue of the AP-2ε^{null} phenotype
169 indicates that our inducible R26AP2ε mouse line is a suitable model for conditional
170 expression of functional AP-2ε.
171
172 **Re-expressing AP-2ε in AP-2ε mice rescues social behaviors**
173 The specification and organization of VSNs and their respective circuit assembly
174 in the AOB are essential to trigger a variety of social and sexual behaviors (Chamero et
175 al., 2011; Chamero et al., 2007; Stowers et al., 2002; Trouillet et al., 2019) . We
176 speculated that AP-2ε^{Null} mice could not discriminate between urine of different sexes.
177 Thus, we performed an odorant preference test. In this test, individual mice were
178 simultaneously presented with male and female whole urine for a two-minute period
179 (Figure 3A). Wild-type mice showed a significant preference for urine from the opposite
180 sex (Figure 3B)(Pankevich et al., 2004; Stowers et al., 2002). However, AP-2ε^{Null} male
181 mice did not display significant preference for female urine, confirming a loss of function
182 (LOF) of basal VSNs (Lin et al., 2018) and consequently a reduced ability to discriminate
183 between urine from either sex (Figure 3B)(Pankevich et al., 2004; Stowers et al., 2002).

184 However, AP-2ε^{Rescue} male mice showed a significant preference for female urine similar
185 to WT controls (Figure 3B).
186 To further investigate the behavioral outcome of AP-2ε LOF and AP-2ε re-
187 expression in AP-2ε^{Null} mice, we performed a resident intruder assay for intermale
188 aggression (Figure 4C)(Chamero et al., 2011; Montani et al., 2013; Stowers et al., 2002).
189 Wild-type male mice showed aggressive behaviors toward intruders upon detecting male
190 specific odorants (Figure 4D). Most AP-2ε^{Null} mice did not attack the intruder (Figure 3D).
191 Yet, when male AP2$\varepsilon^{Cre/Cre}$/R26AP2$\varepsilon^{+/-}$ (AP-2ε^{Rescue}) mice were exposed to male
192 intruders, they displayed aggressive behavior similar to that of controls (Figure 3D). We
193 measured the mass of the seminal vesicles from each genotype to rule out any changes
194 in general androgen levels, which may explain any potential behavioral differences
195 ((Zuloaga et al., 2007)). We found no significant differences when the seminal vesicle
196 weights were normalized to the total body weight of each mouse (Figure 3E). Taken
197 together, these data suggest re-expression of AP-2ε in KO mice can re-establish the
198 functional properties of basal VSNs.
199
200 **Ectopic expression of AP-2ε in mature apical VSNs increases the expression of**
201 **basal specific markers leading to a progressive disorganization of the VNE.**
202 Several AP-2 family members have been proposed to have pioneer activity
203 (Fernandez Garcia et al., 2019; Rothstein and Simoes-Costa, 2020; Seberg et al., 2017;
204 Williams et al., 2009). We tested whether ectopic AP-2ε expression can induce an
205 alternative genetic program in postmitotic neurons. Olfactory marker protein (OMP) is an
206 accepted marker for postmitotic/maturing olfactory and vomeronasal sensory neurons
207 (Buiakova et al., 1994; Enomoto et al., 2011; Farbman and Margolis, 1980). By analyzing
208 our scSeq data from OMPCre$^{+/-}$ mice, we found that OMP mRNA expression in maturing
209 apical neurons begins shortly after the apical basal dichotomy is established (Figure 1E).
210 We concluded that OMP can serve as a suitable genetic entry-point to test whether AP-
211 2ε can redirect apical neurons toward a basal neuron identity. Thus, we used an OMPCre
212 mouse line to drive expression of AP-2ε (OMPCre$^{+/-}$/R26AP2$\varepsilon^{+/-}$) in all olfactory and
213 vomeronasal neurons. In this manuscript we will often refere to OMPCre$^{+/-}$/R26AP2$\varepsilon^{+/-}$ as

214 ectopic mutants. Notably, both apical and basal VSNs express several known Tfap2
215 cofactors, including Cited2 and p300/CBP (Bamforth et al., 2001; Bragança et al., 2003;
216 Eckert et al., 2005)(Supplementary Figure S1) suggesting that both VSN populations are
217 molecularly competent for functional AP-2ε transcriptional activity.

218 Immunostaining against AP-2ε on P10 OMPCre$^{+/-}$ controls showed that AP-2ε
219 expression was limited to basal VSNs with no AP-2ε immunoreactivity in the main
220 olfactory epithelium (OE) (Figure 4A, Figure S2A). However, in OMPCre$^{+/-}$/R26AP2ε$^{+/-}$
221 mutants, we found immunodetectable AP-2ε in the main olfactory epithelium (Figure S2B)
222 and, as expected, in both apical and basal VSNs (Figure 4E). Notably, in OMPCre$^{+/-}$
223 /R26AP2ε$^{+/-}$ mice, we also observed sparse AP-2ε expression in sustentacular cells lining
224 the lumen of the VNO (Figure 4E). These results suggest that OMPCre recombination
225 can also occur in sustentacular cells. OMPCre$^{+/-}$ controls and OMPCre$^{+/-}$/R26AP-2ε$^{+/-}$
226 mutants displayed comparable OE gross morphology (Supplementary Figure S2).
227 Consistent with our observation of no ectopic V2R immunoreactivity in OE mutants
228 (Figure S2D). However, when comparing the VNO of P10 controls and OMPCre$^{+/-}$
229 /R26AP2ε$^{+/-}$ mutants, we observed that OMPCre$^{+/-}$/R26AP-2ε$^{+/-}$ mice had a significantly
230 broader expression of Gαo (Figure 4B,F) and V2R2 (Figure 4C,G), spanning from basal
231 VNO regions to the lumen. scRNA-Seq data from OMPCre$^{+/-}$ controls and OMPCre$^{+/-}$
232 /R26AP2ε$^{+/-}$ confirmed that apical VSNs expressing AP-2ε had variable, but a significant
233 ($P<0.05$) upregulation, of the basal specific markers Gαo and Vmn2r7 (Figure 4, I,J).

234 Analysis at P21 revealed a higher number of individual or small clusters of cells
235 ectopically expressing basal markers in the apical regions (Figure 4O-S). In adult
236 OMPCre$^{+/-}$/R26AP2ε$^{+/-}$ mutants, we noticed an increasing level of cellular disorganization
237 of the VNE with: 1) VSNs spanning from basal territories to regions of the lumen devoid
238 of Sox2+ sustentacular cells, and 2) ectopic sustentacular cells organized in spherical
239 structures or intraepithelial cysts with a subsidiary lumen within apical and basal territories
240 (Figure 5, B-C). Notably, the regions with ectopic sustentacular cells appeared to be
241 mostly surrounded by apical VSNs expressing AP-2ε, Meis2, and Sox2 and were
242 enriched in the intermediate zones of the VNE (Figure 5 B-D). Interestingly, a low level of
243 Sox2 immunoreactivity was observed in Meis2+ VSNs in both controls and OMPCre$^{+/-}$

244 /R26AP2$\varepsilon^{+/-}$ mice with higher intensity in cells closer to the sustentacular cell layer (Figure
245 S3).
246 The affinity and positioning of epithelial cells are largely dictated by the expression
247 of surface adhesion molecules (Fagotto, 2014; Polanco et al., 2021). Transcriptome
248 comparison of OMPCre$^{+/-}$/R26AP2$\varepsilon^{+/-}$ mutants and controls suggest that the aberrant cell
249 positioning in the VNE of mutants can arise from broad variations in expression levels of
250 multiple adhesion molecules throughout Meis2+ cells (Figure 5 E).
251 Furthermore, scRNA-Seq of the adult OMPCre$^{+/-}$/R26AP2$\varepsilon^{+/-}$ allowed us to
252 understand whether sustentacular cells with ectopic AP-2ε expression were contributing
253 to the disorganization of the VNE. By performing differential gene expression analysis on
254 the AP-2ε positive and negative sustentacular cells from the adult OMPCre$^{+/-}$/R26AP2$\varepsilon^{+/-}$
255 mice we observed significantly dysregulated genes (550 upregulated; 571
256 downregulated, adjusted p-value<0.05) with enrichment of genes related to tight-
257 junctions, cell-cell adhesion, and cytoskeletal organization (Figure 3C,D), which may
258 contribute to the disorganized neuroepithelium.
259
260 **AP-2ε can partially reprogram VSN neuronal identity of OMPCre$^{+/-}$ and OMPCre$^{+/-}$**
261 **/R26AP2$\varepsilon^{+/}$**
262 To further elucidate the gene expression changes in Meis2+ VSNs after AP-2ε
263 expression, we analyzed the UMAPs using scSeq from VSNs in controls and mutant
264 mice. These revealed similar clustering at the stages of neurogenesis and differentiation
265 across genotypes (Figure 6A-B). However, control animals showed AP-2ε expression was
266 limited to maturing basal VSNs (Figure 6A'-A'''). In OMPCre$^{+/-}$/R26AP-2$\varepsilon^{+/-}$ mutants,
267 ectopic AP-2ε mRNA was also expressed in maturing and mature apical neurons (Figure
268 5B', B'''). When analyzing the UMAPs, we noticed that mature apical VSNs in the controls
269 formed a distinct and independent cluster (Figure 6A-A'''), while the apical and basal
270 clusters appeared to converge in OMPCre$^{+/-}$/R26AP-2$\varepsilon^{+/-}$ mutants (Figure 6B-B''').
271 To understand the extent to which AP-2ε can reprogram apical VSNs, we
272 compared the expression of the most enriched genes in apical and basal VSNs of
273 OMPCre$^{+/-}$ controls to the apical VSNs of OMPCre$^{+/-}$/R26AP-2$\varepsilon^{+/-}$. Interestingly, this

274 analysis revealed that apical VSNs of OMPCre$^{+/-}$/R26AP-2ε$^{+/-}$ mice had a mixed apical-
275 basal expression profile with a significant down-regulation of ~22% of the apical-enriched
276 genes (7/32), and a significant upregulation of ~28% of the basal-enriched genes (20/71)
277 (Figure 6 C; Supplementary Table S2). Of the aberrantly expressed genes in the apical
278 VSNs of OMPCre$^{+/-}$/R26AP-2ε$^{+/-}$ mice, we identified a reduction in Calreticulin (Calr)
279 mRNA levels together with a strong upregulation of Calreticulin4 (Calr4), which persists
280 in adulthood (Figure 6 D-G, Table S2, Figure S6 A,C)(Dey and Matsunami, 2011). ISH at
281 P11 confirmed that Calr4 is normally expressed by basal VSNs in controls. However, in
282 OMPCre$^{+/-}$/R26AP2ε$^{+/-}$ mutants Calr4 mRNA was found in both apical and basal VSNs
283 (Figure 6D-I). In line with previous studies (Dey and Matsunami, 2011), we found that
284 Calr was expressed below ISH detectability.

285 Axonal projection along the anterior posterior axis of the AOB is determined by
286 axon guidance molecules such as Nrp2, Robo2 while the the coalescence of vomeronasal
287 sensory neuron axons into glomeruli is largely dictated by Kirrel adhesion
288 molecules(Cloutier et al., 2002; Prince et al., 2013; Prince et al., 2009; Vaddadi et al.,
289 2019). Notably, the mRNA expression levels for the guidance receptors, Robo2 and Nrp2,
290 and the adhesion molecules, Kirrel2 and Kirrel3, did not significantly change after ectopic
291 AP-2ε expression. In fact, by immunostaining against Robo2 and Nrp2 we confirmed
292 immunoreactivity of Nrp2 in the anterior and Robo2 in the pAOB similar to controls and
293 observed no significant differences in the average size of anterior or posterior AOB
294 between genotypes (Figure S4 A,B,E). Moreover, quantifications based on Kirrel2 and
295 Kirrel3 immunostaining did not reveal major changes in glomerular size or number in the
296 AOB (Figure S4 C,D,F,G)(Bahreini Jangjoo et al., 2021).

297 Single cell transcriptome analysis of apical and basal neurons of WT controls and
298 OMPCre$^{+/-}$/R26AP2ε$^{+/-}$mutants at P60 highlighted perduring ectopic expression of basal
299 specific genes in apical neurons and downregulation in the expression of apical specific
300 markers including Meis2 (Supplementary Fig S6A,C). At this stage, we observed some
301 aberrant gene expression in the basal OMPCre$^{+/-}$/R26AP-2ε$^{+/-}$ neurons compared to
302 OMPCre$^{+/-}$/R26AP-2ε$^{+/-}$ controls (Figure S6B). These data suggest that AP-2ε can
303 partially reprogram postnatal apical neurons. This prolonged AP-2ε overexpression may
304 trigger a dose dependent effect in gene expression. These data suggest that AP-

305 2ε expression in maturing/mature VSNs is sufficient to upregulate portions of the basal
306 VSN genetic program and repress a portion of the apical VSN genetic program bypassing
307 cellular plasticity restrictions.
308
309 **Identification of direct AP-2ε targets via CUT&RUN**
310 Our findings suggest a key role for AP-2ε in controlling the expression of specific
311 basal specific genes. Transcriptomic studies in AP-2ε^{Null} mice showed loss of expression
312 of basal VSN specific genes suggesting that AP-2ε controls parts of the basal and apical
313 VSN genetic programs (Lin et al., 2018). However, it remains unknown whether AP-2ε
314 regulates VSN genetic programs directly or indirectly. So, we performed genome-wide
315 mapping of transcription factor occupancy with cleavage under targets and release using
316 nuclease (CUT&RUN) to determine the direct genetic targets of AP-2ε in the VNO to pair
317 with our scRNA-Seq (Figure 6J-M). Our analyses identified over 3000 replicable peaks in
318 VNO tissue indicating AP-2ε binding sites (Figure 6J). Of these putative binding sites, we
319 found that 59.1% of the peaks occurred in promoter regions (defined as any region
320 1000bp upstream or 200bp downstream a transcription start site), 19.54% in distal
321 intergenic regions, and ~17.78% in intronic regions (Figure 6H). These results suggest
322 that most AP-2ε activity directly regulates transcription, with perhaps a secondary role in
323 enhancer regions.
324 When we compared AP-2ε direct targets with our identified apical and basal
325 enriched genes from mature VSN populations, we discovered that 15.6% of our identified
326 apical-enriched genes (5/32 genes) (Supplementary Table 1) were AP-2ε direct targets
327 and approximately 27% of our identified basal-enriched genes (21/71 genes) are AP-2ε
328 direct targets (Figure 6H). Of the canonical apical and basal markers and signal
329 transduction machinery only Gαi2/Gnai2 had putative direct AP-2ε occupancy and
330 assumed regulation of transcription (Figure S5C). Notably, our newly discovered list of
331 basal enriched genes (Supplementary Table 1) indicated that only Krt18 showed a
332 putative AP-2ε binding site within its promoter region. As expected from a terminal
333 selector gene, these data suggest that AP-2ε directly binds and regulates batteries of
334 apical and basal enriched genes (Figure S5C).

335 After ectopic AP-2ε expression, only a portion of the apical and basal enriched
336 genes were significantly up/down-regulated. When we compared the AP-2ε direct targets
337 with the statistically significant upregulated and down-regulated genes in the OMPCre$^{+/-}$
338 /R26AP-2ε$^{+/-}$ mutants, we observed that AP-2ε had direct control over several
339 downregulated and upregulated genes (Supplementary Figure S4). These data suggest
340 that AP-2ε plays a dual role in maintaining the basal VSNs' genetic program while
341 restricting the expression of genes normally enriched in apical VSNs (Supplementary Fig
342 S5).
343 Gene Ontology analysis of genes associated with AP-2ε peaks showed an
344 enrichment of factors involved in protein degradation, transcription coregulator activity,
345 and histone and chromatin modification (Supplementary Figure S5A). Motif enrichment
346 analysis of AP-2ε peaks revealed Tfap2 as the top enriched motif (p=1e-180), as
347 expected. Other transcription factor motifs enriched in the same regions as AP-2ε peaks
348 include SP, KLF, EBF, RFX, NRF, DLX, and LHX transcription factor families
349 (Supplementary Fig S4B). As many transcription factors work with other cofactors to
350 regulate gene expression (Huang et al., 2015; Monahan et al., 2017), these motifs may
351 represent potential cofactors that work in concert with AP-2ε to mediate either an
352 activating or repressive role in the VNO.
353
354 **Ectopic AP-2ε does not alter socio-sexual behaviors**
355 To determine whether the aberrant gene expression in apical VSNs could alter
356 VSNs' functions and related social behaviors, we evaluated intermale aggression and
357 odorant preference (Koolhaas et al., 2013). By performing resident intruder tests, we
358 showed that the level of intermale aggression of OMPCre$^{+/-}$/R26AP-2ε$^{+/-}$ male mice
359 trended higher but not significantly different than WT controls (Figure 7G). However,
360 among the animals that displayed aggressive behavior we observed significant increase
361 in the number of attacks from WT to OMPCre$^{+/-}$/R26AP-2ε$^{+/-}$ mutants (p=0.0015;
362 WT=16.00 SE+/- 3.1; Ectopic=43.75 SE+/- 4.8). The odorant preference test in male mice
363 also revealed that OMPCre$^{+/-}$/R26AP-2ε$^{+/-}$ mutants exhibited preferential interest in whole
364 female urine similar to controls (Figure 7H). All together these data suggest that ectopic

365 AP-2ε expression does not disrupt intermale aggression behavior nor sex odorants
366 discrimination in males (Figure 7H). When we tested OMPCre$^{+/-}$/R26AP-2ε$^{+/-}$ females, we
367 observed much more variability in their individual odor preferences compared to controls,
368 even though still retained their preference for opposite sex odorants. These data indicate
369 that ectopic AP-2ε expression in apical VSNs does not dramatically impair sex odorants
370 discrimination.
371
372 **Reduced apical VSNs' activation in response to female specific odorants**
373 Whole male mouse urine activates both V1Rs and V2Rs (Krieger et al., 1999),
374 while female odorants preferentially activate apical VSNs (Dudley and Moss, 1999; Norlin
375 et al., 2001; Silvotti et al., 2018). To determine if OMPCre$^{+/-/}$R26AP-2ε$^{+/-}$ mice had altered
376 chemodetection we quantified VSNs' activation after exposure to either male or female
377 soiled bedding. After exposure to the soiled bedding, brains were collected after 90
378 minutes to allow adequate time for the phosphorylation of the ribosomal protein S6 (pS6)
379 in the VSNs' cell bodies (Silvotti et al., 2018). VSNs activation was quantified after
380 immunostaining against pS6 (Ser 240/244) on coronal sections of the VNO (Figure 6A-
381 D). Apical and basal neurons were identified with Meis2 immunostaining against Meis2
382 and categorized as either pS6+/Meis2+ apical or pS6+/Meis2- basal VSNs (Figure 6A-
383 D). We found that male OMPCre$^{+/-}$/R26AP-2ε$^{+/-}$ mutants had similar patterns of activation
384 to WT controls (Figure 6A,B,E). Notably, we observed a slight but non-significant increase
385 in the number of activated basal VSNs OMPCre$^{+/-}$/R26AP-2ε$^{+/-}$ (Figure 6E). These data
386 suggest that ectopic expression of AP-2ε may enhance the ability of basal VSNs to detect
387 male-specific odorants or the number neurons with basal features.
388 When we exposed OMPCre$^{+/-}$/R26AP-2ε$^{+/-}$ mutants to female odorants, we found
389 an expected selective activation of apical VSNs in WT mice (Silvotti et al., 2018)(Figure
390 7E,F,H). Notably, fewer VSNs from female OMPCreR26AP-2ε mutants were activated
391 than controls when female were exposed to female soiled bedding (Figure 7H). Further
392 analysis showed that while no significant difference in the number of basal VSNs were
393 activated between WT and mutants, there was a dramatic decrease in the number of
394 apical VSNs activated by the female bedding (Figure 7H). These data indicate, as

395 observed after conditional Gαi2 ablation (Trouillet et al., 2019), that LOF of apical VSNs
396 does not translate in major behavioral changes.
397 Interestingly, we also observed that OMPCre$^{+/-}$/R26AP-2ε$^{+/-}$ mutants had pS6
398 immunoreactivity in some sustentacular cells after exposure to male and female soiled
399 bedding that was not present in WT controls (Figure 7E,F). We found no indications that
400 the sustentacular cells gained the ability to detect chemosignals when we did the
401 differential gene expression analysis of sustentacular cells of WT and mutants as we
402 found no significant upregulation of V1R/V2R signal transduction machinery (Gnao1,
403 Gnai2, V1Rs, V2Rs, Trpc2.. Intriguingly, we observed a decrease in genes involved in
404 dephosphorylation (i.e. Ppp1r15a, Ppp2ca, Figure S3) in the mutant sustentacular cells,
405 suggesting that a decrease in phosphatase activity may lead to the sustained
406 phosphorylation of Rps6.
407
408 **DISCUSSION**
409 Understanding how differentiated neurons retain cellular plasticity remains critical
410 to identify how genetic insults can compromise neuronal identity, circuit assembly and
411 function (Hobert and Kratsios, 2019; Molyneaux et al., 2007; Patel and Hobert, 2017;
412 Pereira et al., 2019; Rahe and Hobert, 2019). Spatial and temporal expression of terminal
413 selector genes regulates the establishment and maintenance of neuronal identity remains
414 foundational to elucidate the assembly of functional neuronal circuits (Arlotta et al., 2005;
415 Cau et al., 2002; Cau et al., 1997; Molyneaux et al., 2007). In fact, loss of terminal selector
416 genes can lead to loss of neuronal identity and increase cellular/phenotypic plasticity,
417 while expression of specific TFs can induce specific cellular features only at particular
418 developmental windows (Hobert, 2008; Rahe and Hobert, 2019).
419 Rodents and some marsupials have a binary vomeronasal epithelium where the
420 two main types of VSNs, apical and basal VSNs, are generated throughout life from a
421 common pool of Ascl1 progenitors (Berghard and Buck, 1996; Jia and Halpern, 1996;
422 Katreddi and Forni, 2021; Mohrhardt et al., 2018; Silva and Antunes, 2017; Taroc et al.,
423 2020; Weiler et al., 1999). The generation of these two distinct populations is central for
424 critical socio-sexual behavior in rodents (Oboti et al., 2014; Perez-Gomez et al., 2014). In
425 this study, we used the mouse VNO as a model system and combined scRNA-Seq,

426 histology, behavior, and CUT&RUN methodologies to show that the TF AP-2ε is a basal
427 VSN specific terminal selector gene capable of partially reprogramming the apical VSN
428 identity.

429 Using scRNA-Seq, we discovered key transcriptomic differences between mature
430 basal and apical VSNs that were previously unreported (Figure 1J, Supplementary Table
431 S1). We also demonstrated that AP-2ε mRNA is restricted to maturing Gαo/basal VSNs
432 (Figure 1G) and that AP-2ε itself does not initiate the basal VSN differentiation program,
433 but rather maintains the integrity of the basal neuronal identity. We discovered that AP-
434 2ε is indispensable for normal territorial and sex-preference behaviors by reestablishing
435 AP-2ε expression in AP-2ε KOs. We also elucidated that it acts in controlling VSN gene
436 expression through activating and repressive activity when analyzing mature/maturing
437 Meis2+ apical VSNs in OMPCre$^{+/-}$/R26AP-2ε$^{+/-}$ mutant mice.

438 During differentiation chromatin barriers dynamically restrict the cellular plasticity
439 that prevents ectopic terminal selector genes from genetically reassigning neurons (Rahe
440 and Hobert, 2019). We previously demonstrated in AP-2ε KOs that postmitotic VSNs can
441 deviate from the basal differentiation program and turn on sets of apical specific genes,
442 but AP-2ε LOF did not prevent basal neurons from acquiring basal features, such as Gαo
443 or V2Rs (Lin et al., 2018). These data suggested that AP-2ε activity is crucial to restrict
444 basal VSN phenotypic plasticity (Lin et al., 2018). Here we showed that AP-2ε null mice
445 display reduced odorant sex preference and intermale aggressive behavior, which are
446 classic phenotypes related to basal VSN LOF (Stowers et al., 2002). However, we found
447 that reintroducing AP-2ε in maturing basal AP-2ε KO neurons was sufficient to rescue
448 cellular homeostasis, physiological functions, and related behavior.

449 Terminal selectors define neuronal identity by suppressing alternative programs
450 and can also act as pioneer factors (Lupien et al., 2008; Magnani et al., 2011; Mangale
451 et al., 2008). Based on our data, we conclude that AP-2ε can partially reprogram the
452 transcriptome of differentiated cells, as expected from a pioneer factor and other
453 members of the Tfap2 family (Rothstein and Simoes-Costa, 2020). When we used
454 OMPCre drivers to induce ectopic AP-2ε in differentiated olfactory and vomeronasal
455 neurons, we observed progressive gene and morphological changes in the VNO, but no

456 gross morphological changes in the main olfactory epithelium. We suspect the lack of
457 phenotype in the OE may arise from the absence of necessary Tfap2 cofactors , that are
458 expressed in the VNO (Figure S1, (Eckert et al., 2005)).

459 The co-expression of AP-2ε in Meis2+ apical VSNs in OMPCre$^{+/-/}$R26AP-2ε$^{+/-}$ mice
460 revealed that Meis2 and most apical specific genes showed comparable expression
461 levels between controls and mutant animals at P10 (Figure 5A-B). However, single-cell
462 transcriptome analyses in adult mice indicated that several apical genes including Meis2,
463 were expressed at significantly lower levels than controls (Figure S6 A,C). These data
464 suggest that AP-2ε acts as a terminal selector protein that negatively affects a portion of
465 the apical program.

466 Ectopic expression of individual terminal selector genes selectively can control
467 specific molecular features linked to neuronal function and identity, but not pan-neuronal
468 features like guidance cue receptors (Patel and Hobert, 2017; Stefanakis et al., 2015).
469 Single-cell RNA-Seq revealed that AP-2ε ectopic expression, surprisingly, does not alter
470 the expression of VSN-specific guidance cue receptors Nrp2 and Robo2 (Cho et al., 2011;
471 Prince et al., 2009; Walz et al., 2002) (Cloutier et al., 2002). Changes in Kirrel2 and Kirrel3
472 expression were not statistically significant. In accord with this, we did not find obvious
473 changes in glomeruli size or number in the AOB (Figure S4 C,D,F,G).

474 In OMPCre$^{+/-}$/R26AP-2ε$^{+/-}$ mutants, we observed that the cellular organization and
475 lamination of the vomeronasal epithelium became severely disrupted between P10 and
476 adult ages. Notably, we found in mutants basal neurons located at the level of the VNE
477 lumen and ectopic sustentacular cells forming intraepithelial cyst-like structures in both
478 apical and basal territories (Figure 5B,C). Notably, the disorganization of the VNE that
479 resembles intraepithelial cysts as previously described in aging mice (Wilson and
480 Raisman, 1980), appeared to be more pronounced/frequent in regions proximal to the
481 neurogenic marginal zones (Figure 5D,E), where OMP mRNA is expressed following
482 Gap43 expression. Therefore, we posit that the regionalization of the VNE phenotypes
483 might represent cells that underwent AP-2ε ectopic expression at early maturation stages.
484 When we compared mRNA of control and ectopic AP-2ε mutants, which have
485 disorganized VNE, we observed changes in expression levels of many surface and cell
486 adhesion related molecules as well as upregulation of stress related genes (Figure 5F,

487 S3E). In addition to this, scRNA-seq analysis of AP-2ε positive and negative sustentacular
488 cells in adult OMPCre$^{+/-}$/R26AP-2ε$^{+/-}$ mutants revealed massive changes in gene
489 expression in these support cells. Future studies should focus on understanding which of
490 the dysregulated genes in VSNs and sustentacular cells contribute to the cytoarchitectural
491 organization of VSNs and sustentacular cells.

492 To elucidate the mechanism of action of AP-2ε, we performed CUT&RUN (Skene
493 et al., 2018; Skene and Henikoff, 2017). This analysis identified putative direct targets of
494 AP-2ε and showed 3000+ putative binding sites in the vomeronasal tissue. Of these, we
495 found that most of binding sites were primarily in promoter regions, not in intergenic and
496 intronic regions. These data suggest that AP-2ε's main mechanism of action directly
497 regulates gene transcription with perhaps a secondary role at enhancer regions. We
498 found AP-2ε bound to the up and down-regulated genes in both apical VSNs and
499 sustentacular cells in the OMPCre$^{+/-/}$R26AP-2ε$^{+/-}$ ectopic mouse line, which suggests that
500 AP-2ε can act as both a transcriptional activator and repressor. Motif analysis of these up
501 and downregulated regions indicates that AP-2ε may function in concert with specific
502 transcriptional cofactors to fulfill a dual role in maintaining the basal VSN genetic program
503 and restricting cellular plasticity. Notably our CUT&RUN data showed an enrichment of
504 factors involved in transcription coregulator activity, histone modification, and chromatin
505 modification (Figure S5 A). These data suggest that AP-2ε may play a role in modifying
506 the chromatin landscape indirectly or in tandem with these transcriptional cofactors to
507 regulate the basal genetic program. Even though transcriptome and histological analysis
508 of the VNE showed significant changes in canonical apical and basal specific genes, only
509 Gαi2 and Krt18 had AP-2ε peak assignments, suggesting that AP-2ε acts indirectly to
510 regulate these genes. However, since peaks were assigned to the nearest gene, we
511 cannot exclude long-distance gene regulation through enhancer regions as a contributor.

512 Sex odorants activate different sets of vomeronasal receptors and therefore
513 different populations of VSNs (Dudley and Moss, 1999; Keller et al., 2006; Silvotti et al.,
514 2018). Interestingly, scRNA-seq analysis and validation via ISH revealed that ectopic AP-
515 2ε in mature apical VSNs had upregulated Calreticulin-4 (Calr4) ER chaperone proteins,
516 which has been previously shown to increase V2R cell surface expression (Dey and

517 Matsunami, 2011). These data suggest that ectopic AP-2ε in mature apical VSNs may
518 indirectly disturb vomeronasal receptor expression or insertion and therefore alter the
519 ability of VSNs to detect and process sex-specific odorants.

520 Using pS6 immunoreactivity on activated VSNs after male odorant exposure
521 indicated a potential sensitization of basal VSNs and unchanged activation of apical VSNs
522 after ectopic AP-2ε expression. Conditional ablation of normal apical VSN signal
523 transduction does not undermine intermale aggression, rather it enhances territorial
524 aggression in mutant males (Trouillet et al., 2019). In line with this, we found that
525 OMPCre$^{+/-}$/R26AP-2ε$^{+/-}$ mutants that display aggressive behavior had higher levels of
526 aggression towards male intruders when compared to WT controls. However, the
527 nonsignificant changes in pS6 activation after male odorant exposure suggest that the
528 LOF in apical VSNs might occur in processing or signaling rather than detection of stimuli.
529 These data indicate that ectopic AP-2ε expression is sufficient to subvert the function of
530 apical VSNs and therefore alter intrinsic social behaviors.

531 Strikingly, female OMPCre$^{+/-}$/R26AP-2ε$^{+/-}$ showed significantly decreased
532 activation of apical VSNs in response to female bedding compared to controls. In rodents,
533 olfactory sex discrimination persists after VNO excision; however, preference for opposite
534 sex odorants is mediated by the accessory olfactory system (Keller et al., 2006;
535 Pankevich et al., 2004). Despite the putative desensitization of the apical VSNs in
536 OMPCre$^{+/-}$/R26AP-2ε$^{+/-}$ mutants, transcriptome and morphological changes in the VNO
537 did not compromise normal sex odorant preference in male or female mutants. In fact,
538 conditional ablation of Gαi2, which is required for normal signaling of apical VSNs, did
539 not alter normal male sexual behavior, including male preference for estrous female urine
540 (Trouillet et al., 2019). Together, these data indicate that though ectopic AP-2ε expression
541 in apical VSNs subverts the function of apical VSNs it does not alter normal sex
542 identification and territorial behaviors (Trouillet et al., 2019) , confirming a dispensable
543 role for these neurons in the tested behaviors.

544 In conclusion, the results of our study indicate that AP-2ε has many features of a
545 terminal selector gene with roles in controlling the expression of several basal VSN genes
546 and repressing apical ones, which is necessary for normal basal VSN functions that
547 mediate territorial and sex preference behaviors in mice. We showed that AP-2ε has an

548 extraordinary ability in reprogramming the transcriptome of postnatal VSNs in rodents and
549 confers an ambiguous transcriptome identity to these cells bypassing cellular plasticity
550 restrictions over time.
551 Our study suggests that as previously hypothesized by others (Hobert and
552 Kratsios, 2019; Rahe and Hobert, 2019) aberrant expression of terminal selector genes
553 in postnatal cells can alter the organization of a neuroepithelium, the transcriptomic
554 identity of neurons and lead to neuronal pathologies.
555

556 **ACKNOWLEDGEMENTS**

557 ***Funding***
558 This publication was supported by the National Institutes of Health (NIH) by the
559 Eunice Kennedy Shriver National Institute of Child Health and Human Development of
560 the National Institutes of Health under the Awards R15-HD096411 (P.E.F) and R01-
561 HD097331/HD/NICHD (P.E.F), the National Institute of Deafness and Other
562 Communication Disorders of the National Institutes of Health under the Award R01-
563 DC017149 (P.E.F), the National Institute of Dental and Craniofacial Research under the
564 Award R01DE028576 (M.S.-C), and the National Institute of Mental Health under the
565 Award R15-MH118692 (D.G.Z).
566

567 **STAR★METHODS**

568

569 **KEY RESOUCES TABLE**

570

571

572 **RESOURCE AVAILABILITY**

573

574 ***Lead contact***
575 Further information and requests for resources and reagents should be directed to
576 and will be fulfilled by the lead contact, Paolo E. Forni (pforni@albany.edu).
577

578 ***Materials availability***

579 Mouse lines generated in this study will be deposited to Jackson Labs by the time
580 of publication.
581 There are restrictions in availability of the antibody Rabbit anti-V2R2 which was
582 obtained from the lab of Roberto Tirindelli (University of Parma, Italy) and is not
583 commercially available.
584
585 ***Data and code availability***
586 The Single-cell RNA-sequencing and CUT& RUN sequencing data discussed in
587 this publication have been deposited at NCBI's Gene Expression Omnibus and are
588 publicly available as of the date of publication. Accession numbers are listed in the key
589 resources table. This paper reports no original code. Any additional information required
590 to reanalyzed the data reported in this paper is available from the lead contact upon
591 request.
592
593 **EXPERIMENTAL MODEL AND SUBJECT DETAILS**
594
595 ***Animals***
596 The R26AP2ε mice were produced by Cyagen (Santa Clara, CA). on a C57B/6
597 background. The AP-2εCre line (*Tfap2e*$^{tm1(cre)Will}$) was obtained from Dr. Trevor Williams,
598 Department of Craniofacial Biology, University of Colorado. The R26AP-2ε (B6.Cg-
599 Gt(ROSA)26Sor$^{tm(CAG\text{-}mTfap2e)For}$) mouse line was produced through Cyagen on a C56BL/6
600 background. The OMPCre line (B6;129P2-*Omp*$^{tm4(cre)Mom}$/MomJ) was obtained from Dr.
601 Paul Feinstein (Hunter College, City University of New York) on a 129P2/OlaHsd
602 background and backcrossed to a C57BL/6 background for 6 generations at the time of
603 this study. The characterization and comparison of the rescue of the AP-2ε phenotype
604 (AP-2εCreR26AP-2ε), AP-2ε KO, and wild-types were performed on a C57BL/6
605 background. OMPCre$^{+/-}$/R26AP2ε$^{+/-}$ mutant mice are viable. Genotyping of mutants was
606 performed by PCR. Primers used are detailed in the Key Resources Table.
607 Mice were housed under a 12hr day/night cycle. Animals were collected/analyzed
608 at P10, P21, and Adult (P60-P90) ages. For all morphological analyses both males and
609 females were included unless otherwise specified. All mouse studies were approved

610 by the University at Albany Institutional Animal Care and Use Committee (IACUC). Mouse
611 lines generated in this study will be deposited to Jackson Labs by the time of publication.
612
613 **METHOD DETAILS**
614 ***Generation of the AP-2ε conditional Knock-In Model***
615 The AP-2ε conditional Knock-In allele was generated by targeting the ROSA26
616 gene in C57BL/6 ES cells. The "CAG-loxP-stop-loxP-mouse Tfap2e CDS-polyA" cassette
617 was cloned into intron 1 of ROSA26 in the reverse orientation. In the targeting vector, the
618 positive selection marker (Neo) was flanked by SDA (self-deletion anchor) site, and DTA
619 was used for negative selection. Mouse genomic fragments containing homology arms
620 (Has) were amplified from BAC clone by using high fidelity Taq DNA polymerase and
621 were sequentially assembled into a targeting vector together with recombination sites and
622 selection markers.
623 The ROSA26 targeting construct was linearized by restriction digestion with AscI
624 followed by phenol/chloroform extraction and ethanol precipitation. The linearized vector
625 was transfected into C57BL/6 ES cells according to Taconic-Cyagen's standard
626 electroporation procedures and G418 resistant clones were selected for 24 hours post-
627 electroporation. These were then screened for homologous recombination by PCR and
628 characterized by Southern Blot analysis. Two separate clones, A2 and H2, were
629 successfully transmitted to germline and characterized.
630 Genotyping for the R26AP-2ε mouse line was performed by PCR using R26-AP-
631 2e Common (5' GGAGGGGGGCTCTGAGAT 3'), R26-AP-2e Mutant (5'
632 GGCTGGTGTGGCCAATGC 3'), R26-AP-2e WT (5' GTCGTGAGGCTGCAGGTC 3')
633 with expected bands at 552bp (Mutant) and 400bp (WT).
634
635 ***Resident Intruder Test***
636 The resident intruder assay was used to evaluate aggression in male mice of
637 mutants and controls. Test subjects were housed with intact females for at least one week
638 prior to testing. On the day of testing, all subjects (residents and intruders) were
639 acclimated to the experimental environment for at least 30 minutes prior to the assay.
640 Females were removed immediately before testing. Castrated C57B mice were swabbed

641 with male whole urine immediately before being introduced into the resident male's home
642 cage. Interactions between isolated residents and intruders were recorded for 10min and
643 videos were evaluated using ButtonBox v.5.0 (Behavioral Research Solutions, Madison
644 WI, USA) software for the number and duration of attacks.
645
646 ***Innate olfactory preference test***
647 Adult mice were isolated for at least one week prior to testing. Individual mice were
648 habituated to the experimental environment for at least 30 minutes, then to the test cage
649 for an additional 2 minutes. After the habituation period, cotton swabs scented with either
650 male or female whole urine was placed on either side of the test cage. The time spent
651 sniffing each odorant was normalized to total investigation time.
652
653 ***Neuronal activation in response to sex-specific odorants***
654 Adult mice were isolated for at least one week prior to exposure to either soiled
655 bedding from male or female mice for ~90min then perfused with PBS and 3.7%
656 formaldehyde in PBS, then collected to evaluate neuronal activation with
657 immunohistochemistry against pS6.
658
659 ***Tissue Preparation***
660 Tissue collected at ages ≥P10 were perfused with PBS then 3.7% formaldehyde
661 in PBS. Brain tissue was isolated at the time of perfusion and then immersion-fixed for 3-
662 4 hours at 4°C. Noses were immersion fixed in 3.7% formaldehyde in PBS at 4°C
663 overnight and then decalcified in 500mM EDTA for 3-4 days. All samples were
664 cryoprotected in 30% sucrose in PBS overnight at 4°C, followed by embedding in Tissue-
665 Tek O.C.T. Compound (Sakura Finetek USA, Inc., Torrance CA) using dry ice, and stored
666 at -80°C. Tissue was cryosectioned using a CM3050S Leica cryostat at 16μm for VNOs
667 and 20μm for brain tissue and collected on VWR Superfrost Plus Micro Slides (Radnor,
668 PA) for immunostaining and in situ hybridization (ISH). All slides were stored at -80°C
669 until ready for staining.
670
671 ***Immunohistochemistry***

672 For immunohistochemistry and immunofluorescence antigen retrieval was
673 performed on slides that were submerged in citrate buffer (pH 6.0) above 95°C for at least
674 15min before cooling to room temperature, then permeabilized with and blocked in horse
675 serum based blocking solution before transferring into primary antibodies overnight at
676 4°C. For immunohistochemistry slides were additionally incubated in an H_2O_2 solution
677 (35mL PBS+ 15mL 100% Methanol + 500μL 30% H_2O_2) after antigen retrieval.
678 For chromogen-based reactions, staining was visualized with the Vectastain ABC
679 Kit (Vector, Burlingame, CA) using diaminobenzidine (DAB) (Forni et al., 2011); sections
680 were counterstained with methyl green and mounted with Sub-X mounting medium. For
681 immunofluorescence species-appropriate secondary antibodies conjugated with either
682 Alexa Fluor 488, Alexa Fluor 594, Alexa Fluor 568, Alexa Fluor 680 were used for
683 immunofluorescence detection (Molecular Probes and Jackson ImmunoResearch
684 Laboratories, Inc., Westgrove, PA). Sections were counterstained with 4',6'-diamidino-2-
685 phenylindole (DAPI) (1:3000; Sigma-Aldrich), and coverslips were mounted with
686 FluoroGel (Electron Microscopy Services, Hatfield, PA).
687 Confocal microscopy pictures were taken on a Zeiss LSM 710 microscope.
688 Epifluorescence pictures were taken on a Leica DM4000 B LED fluorescence microscope
689 equipped with a Leica DFC310 FX camera. Images were further analyzed using
690 FIJI/ImageJ software. Antibodies and concentrations used in this study are detailed in the
691 Key Resources Table.
692
693 ***In Situ Hybridization***
694 Digoxigenin-labeled RNA probes were prepared by *in vitro* transcription (DIG RNA
695 labeling kit; Roche Diagnostics, Basel, Switzerland). In situ hybridizations were performed
696 on 16μm cryosections that were rehydrated in 1x PBS for 5min, fixed in 4% PFA in 0.1M
697 phosphate buffer for 20min at 4°C, treated with 10μg/mL proteinase K (Roche) for 12min
698 at 37°C, and then refixed in 4% PFA at 4°C for 20min. To inactivate the internal alkaline
699 phosphatase, the tissue was treated with 0.2M HCl for 30min. Nonspecific binding of the
700 probe to slides was reduced by dipping slides in 0.1M triethanolamine (pH 8.0)/0.25%
701 acetic anhydride solution, then washed with 2x Saline-Sodium Citrate (SSC) buffer before
702 incubating in hybridization solution for 2hrs at room temperature. Slides were then

703 hybridized with 200μl of probe in hybridization solution at 65°C overnight in a moisture
704 chamber. After hybridization, the slides were washed in 2x SSC, briefly, then in 1x
705 SSC/50% formamide for 40min at 65°C. RNase A treatment (10μg/mL) was carried out
706 at 37°C for 30min. The slides were then washed with 2x SSC then 0.2x SSC for 15min
707 each at 65°C. Hybridization was visualized by immunostaining with an alkaline
708 phosphatase conjugated anti-DIG (1:1000), and NBT/BCIP developer solution (Roche
709 Diagnostics). After color reaction, the slides were put into 10mM Tris-HCl pH 8.0/1mM
710 EDTA, rinsed in PBS and air dried before mounting with Sub-X mounting medium.
711
712 ***Single-Cell RNA Sequencing***
713 The vomeronasal organs of OMPCre$^{+/-}$ at P10 and OMPCre$^{+/-}$/R26AP2ε$^{+/-}$ at P10 and
714 3mo were isolated and dissociated into single-cell suspension using neural isolation
715 enzyme/papain (NIE/Papain in Neurobasal Medium with 0.5mg/mL Collagenase A,
716 1.5mM L-cysteine and 100U/mL DNAse I) incubated at 37ºC. The dissociated cells were
717 then washed with HBSS and reconstituted in cell freezing medium (90% FBS, 10%
718 DMSO). Cells were frozen from room temperature to -80ºC at a -1°C/min freeze rate.
719 Single cell suspension was sent to SingulOmics for high-throughput single-cell gene
720 expression profiling using the 10x Genomics Chromium Platform. Data were analyzed
721 along with using Seurat 4.0.5. The scRNA-seq data discussed in this publication have
722 been deposited in NCBI's Gene Expression Omnibus and are accessible through GEO
723 series accession number GSE192746
724 (https://www.ncbi.nlm.nih.gov/geo/query/acc.cgi?acc=GSE192746). We also utilized
725 previously published data from (Katreddi et al., 2021), available through GEO series
726 accession number GSE190330
727 (https://www.ncbi.nlm.nih.gov/geo/query/acc.cgi?acc=GSE190330).
728
729 ***CUT&RUN***
730 Cells frozen in 90% FBS/10%DMSO were thawed at 37°C and resuspended in
731 CUT&RUN wash buffer (20mM HEPES pH7.5, 150mM NaCl, 0.5mM spermidine, plus
732 Roche Complete Protease inhibitor, EDTA-free). CUT&RUN experiments were
733 performed as previously described (Meers et al., 2019) with minor modifications. 0.025%

734 digitonin was used for the Dig-wash buffer formulation. Antibody incubation was
735 performed overnight at 4°C, followed by Protein A-MNase binding for 1 hour at 4°C. Prior
736 to targeted digestion, cell-bead complexes were washed in low-salt rinse buffer (20mM
737 HEPES pH7.5, 0.5mM spermidine, 0.025% digitonin, plus Roche Complete Protease
738 inhibitor, EDTA-free) followed by targeted digestion in ice-cold high-calcium incubation
739 buffer (3.5 mM HEPES pH 7.5, 10 mM $CaCl_2$, 0.025% Digitonin) for 30 minutes at 0°C.
740 Targeted digestion was halted by replacing the incubation buffer with EGTA-STOP buffer
741 (170 mM NaCl, 20 mM EGTA, 0.025% digitonin, 20 µg/ml glycogen, 25 µg/ml RNase A),
742 followed by chromatin release and DNA extraction. Protein AG–MNase was kindly
743 provided by Dr. Steve Henikoff. A rabbit polyclonal Anti-TFAP2E antibody (Proteintech
744 25829-1-AP) was used at a concentration of 1:50 for CUT&RUN experiments.
745
746 ***CUT&RUN library preparation***
747 CUT&RUN libraries were prepared using the NEBNext ultra II DNA library prep kit (New
748 England Biolabs E7645). Quality control of prepared libraries was conducted using an
749 ABI 3730xl DNA analyzer for fragment analysis. Libraries were pooled to equimolar
750 concentrations and sequenced with paired-end 37-bp reads on an Illumina NextSeq 500
751 instrument.
752
753 **QUANTIFICATION AND STATISTICAL ANALYSIS**
754
755 ***Quantification and statistical analyses of microscopy data.***
756 All data were collected from mice kept under similar housing conditions in transparent
757 cages on a normal 12 hr. light/dark cycle. Tissue collected from either males or females
758 in the same genotype/treatment group were analyzed together unless otherwise stated.
759 Ages analyzed are indicated in text and figures. The data are presented as mean ± SEM.
760 Prism 9.2.0 was used for statistical analyses, including calculation of mean values, and
761 standard errors. Two-tailed, unpaired t-test were used for all statistical analyses, and
762 calculated p-values <0.05 were considered statistically significant. Sample sizes and p-
763 values are indicated as single points in each graph and/or in figure legends.

764 Measurements of VNE and cell counts were performed on confocal images or
765 bright field images of coronal serial sections immunostained or in situ hybridizations for
766 the indicated targets. In animals ≥P15, the most central 6-8 sections on the rostro-caudal
767 axis of the VNO were quantified and averaged, and in animals ≥P0, the most medial 4-6
768 sections were quantified and averaged. Measurements and quantifications were
769 performed using ImageJ 2.1.0 and Imaris. Statistical differences between genotypes were
770 quantified with two-tailed unpaired t-test using Prism 9.2.0, (GraphPad Software, CA,
771 USA). Microscopy data reported in this paper will be shared by the lead contact upon
772 request.
773
774 ***CUT&RUN data analysis***
775 In processing CUT&RUN data, paired-end sequencing reads were trimmed using
776 Cutadapt t(Martin, 2011) using the following arguments: "-a
777 AGATCGGAAGAGCACACGTCTGAACTCCAGTCA -A
778 AGATCGGAAGAGCGTCGTGTAGGGAAAGAGTGT --minimum-length=25". Reads
779 were aligned to the reference mouse mm10 assembly from the UCSC genome browser
780 using Bowtie 2 (Langmead and Salzberg, 2012) using the following arguments: "--local -
781 -very-sensitive-local --no-unal --no-mixed --no-discordant -I 10 -X 1000". BAM files were
782 filtered with SAMtools to discard unmapped reads, those which were not the primary
783 alignment, reads failing platform/vendor quality checks, and PCR/optical duplicates (-f 2
784 -F 780). Peak calling was performed using MACS2 (Zhang et al., 2008). Peak-gene
785 annotation was done by mapping peaks to their closest annotated gene using the
786 ChIPseeker R package(Yu et al., 2015). GO term analysis was performed in R using
787 clusterProfiler (Yu et al., 2012). Motif enrichment analysis was performed using HOMER
788 (Heinz et al., 2010). The data from this CUT&RUN experiment has been deposited into
789 the NCBI's Expression Omnibus and are accessible through GEO series accession
790 number GSE193139
791 (https://www.ncbi.nlm.nih.gov/geo/query/acc.cgi?acc=GSE193139).
792
793
794

REFERENCES

Arlotta, P., Molyneaux, B.J., Chen, J., Inoue, J., Kominami, R., and Macklis, J.D. (2005). Neuronal subtype-specific genes that control corticospinal motor neuron development in vivo. Neuron *45*, 207-221.

Bahreini Jangjoo, S., Lin, J.M., Etaati, F., Fearnley, S., Cloutier, J.-F., Khmaladze, A., and Forni, P.E. (2021). Automated quantification of vomeronasal glomeruli number, size, and color composition after immunofluorescent staining. Chemical senses.

Bamforth, S.D., Bragança, J., Eloranta, J.J., Murdoch, J.N., Marques, F.I.R., Kranc, K.R., Farza, H., Henderson, D.J., Hurst, H.C., and Bhattacharya, S. (2001). Cardiac malformations, adrenal agenesis, neural crest defects and exencephaly in mice lacking Cited2, a new Tfap2 co-activator. Nature genetics *29*, 469-474.

Bassett, E.A., Korol, A., Deschamps, P.A., Buettner, R., Wallace, V.A., Williams, T., and West-Mays, J.A. (2012). Overlapping Expression Patterns and Redundant Roles for AP-2 Transcription Factors in the Developing Mammalian Retina. Developmental dynamics : an official publication of the American Association of Anatomists *241*, 814-829.

Berghard, A., and Buck, L.B. (1996). Sensory transduction in vomeronasal neurons: evidence for G alpha o, G alpha i2, and adenylyl cyclase II as major components of a pheromone signaling cascade. The Journal of Neuroscience *16*, 909-918.

Bragança, J., Eloranta, J.J., Bamforth, S.D., Ibbitt, J.C., Hurst, H.C., and Bhattacharya, S. (2003). Physical and functional interactions among AP-2 transcription factors, p300/CREB-binding protein, and CITED2. The Journal of biological chemistry *278*, 16021-16029.

Buiakova, O.I., Krishna, N.S., Getchell, T.V., and Margolis, F.L. (1994). Human and rodent OMP genes: conservation of structural and regulatory motifs and cellular localization. Genomics *20*, 452-462.

Cau, E., Casarosa, S., and Guillemot, F. (2002). Mash1 and Ngn1 control distinct steps of determination and differentiation in the olfactory sensory neuron lineage. Development *129*, 1871-1880.

Cau, E., Gradwohl, G., Fode, C., and Guillemot, F. (1997). Mash1 activates a cascade of bHLH regulators in olfactory neuron progenitors. Development *124*, 1611-1621.

Chambers, B.E., Gerlach, G.F., Clark, E.G., Chen, K.H., Levesque, A.E., Leshchiner, I., Goessling, W., and Wingert, R.A. (2019). Tfap2a is a novel gatekeeper of nephron differentiation during kidney development. Development *146*, dev172387.

Chamero, P., Katsoulidou, V., Hendrix, P., Bufe, B., Roberts, R., Matsunami, H., Abramowitz, J., Birnbaumer, L., Zufall, F., and Leinders-Zufall, T. (2011). G protein G(alpha)o is essential for vomeronasal function and aggressive behavior in mice. Proc Natl Acad Sci U S A *108*, 12898-12903.

Chamero, P., Marton, T.F., Logan, D.W., Flanagan, K., Cruz, J.R., Saghatelian, A., Cravatt, B.F., and Stowers, L. (2007). Identification of protein pheromones that promote aggressive behaviour. Nature *450*, 899-902.

Cho, J.H., Prince, J.E., Cutforth, T., and Cloutier, J.F. (2011). The pattern of glomerular map formation defines responsiveness to aversive odorants in mice. The Journal of neuroscience : the official journal of the Society for Neuroscience *31*, 7920-7926.

839 Cloutier, J.F., Giger, R.J., Koentges, G., Dulac, C., Kolodkin, A.L., and Ginty, D.D. (2002).
840 Neuropilin-2 mediates axonal fasciculation, zonal segregation, but not axonal
841 convergence, of primary accessory olfactory neurons. Neuron *33*, 877-892.
842 de la Rosa-Prieto, C., Saiz-Sanchez, D., Ubeda-Banon, I., Argandona-Palacios, L.,
843 Garcia-Munozguren, S., and Martinez-Marcos, A. (2010). Neurogenesis in subclasses of
844 vomeronasal sensory neurons in adult mice. Developmental neurobiology *70*, 961-970.
845 Dey, S., and Matsunami, H. (2011). Calreticulin chaperones regulate functional
846 expression of vomeronasal type 2 pheromone receptors. Proc Natl Acad Sci U S A *108*,
847 16651-16656.
848 Dudley, C.A., and Moss, R.L. (1999). Activation of an anatomically distinct subpopulation
849 of accessory olfactory bulb neurons by chemosensory stimulation. Neuroscience *91*,
850 1549-1556.
851 Dulac, C., and Axel, R. (1995). A novel family of genes encoding putative pheromone
852 receptors in mammals. Cell *83*, 195-206.
853 Eckert, D., Buhl, S., Weber, S., Jager, R., and Schorle, H. (2005). The AP-2 family of
854 transcription factors. Genome biology *6*, 246.
855 Enomoto, T., Ohmoto, M., Iwata, T., Uno, A., Saitou, M., Yamaguchi, T., Kominami, R.,
856 Matsumoto, I., and Hirota, J. (2011). Bcl11b/Ctip2 controls the differentiation of
857 vomeronasal sensory neurons in mice. The Journal of neuroscience : the official journal
858 of the Society for Neuroscience *31*, 10159-10173.
859 Fagotto, F. (2014). The cellular basis of tissue separation. Development *141*, 3303-3318.
860 Farbman, A.I., and Margolis, F.L. (1980). Olfactory marker protein during ontogeny:
861 immunohistochemical localization. Dev Biol *74*, 205-215.
862 Feng, W., Simoes-de-Souza, F., Finger, T.E., Restrepo, D., and Williams, T. (2009).
863 Disorganized olfactory bulb lamination in mice deficient for transcription factor AP-
864 2epsilon. Mol Cell Neurosci *42*, 161-171.
865 Feng, W., and Williams, T. (2003). Cloning and characterization of the mouse AP-2
866 epsilon gene: a novel family member expressed in the developing olfactory bulb. Mol Cell
867 Neurosci *24*, 460-475.
868 Fernandez Garcia, M., Moore, C.D., Schulz, K.N., Alberto, O., Donague, G., Harrison,
869 M.M., Zhu, H., and Zaret, K.S. (2019). Structural Features of Transcription Factors
870 Associating with Nucleosome Binding. Molecular cell *75*, 921-932 e926.
871 Forni, P.E., Fornaro, M., Guenette, S., and Wray, S. (2011). A role for FE65 in controlling
872 GnRH-1 neurogenesis. The Journal of neuroscience : the official journal of the Society
873 for Neuroscience *31*, 480-491.
874 Heinz, S., Benner, C., Spann, N., Bertolino, E., Lin, Y.C., Laslo, P., Cheng, J.X., Murre,
875 C., Singh, H., and Glass, C.K. (2010). Simple combinations of lineage-determining
876 transcription factors prime cis-regulatory elements required for macrophage and B cell
877 identities. Molecular cell *38*, 576-589.
878 Herrada, G., and Dulac, C. (1997). A novel family of putative pheromone receptors in
879 mammals with a topographically organized and sexually dimorphic distribution. Cell *90*,
880 763-773.
881 Hobert, O. (2008). Regulatory logic of neuronal diversity: terminal selector genes and
882 selector motifs. Proc Natl Acad Sci U S A *105*, 20067-20071.
883 Hobert, O., and Kratsios, P. (2019). Neuronal identity control by terminal selectors in
884 worms, flies, and chordates. Curr Opin Neurobiol *56*, 97-105.

885 Huang, Y.H., Jankowski, A., Cheah, K.S., Prabhakar, S., and Jauch, R. (2015). SOXE
886 transcription factors form selective dimers on non-compact DNA motifs through
887 multifaceted interactions between dimerization and high-mobility group domains.
888 Scientific reports *5*, 10398.
889 Isogai, Y., Si, S., Pont-Lezica, L., Tan, T., Kapoor, V., Murthy, V.N., and Dulac, C. (2011).
890 Molecular organization of vomeronasal chemoreception. Nature *478*, 241-245.
891 Jia, C., and Halpern, M. (1996). Subclasses of vomeronasal receptor neurons: differential
892 expression of G proteins (Gi alpha 2 and G(o alpha)) and segregated projections to the
893 accessory olfactory bulb. Brain research *719*, 117-128.
894 Kantarci, H., Edlund, R.K., Groves, A.K., and Riley, B.B. (2015). Tfap2a Promotes
895 Specification and Maturation of Neurons in the Inner Ear through Modulation of Bmp, Fgf
896 and Notch Signaling. PLoS genetics *11*, e1005037.
897 Katreddi, R.R., and Forni, P.E. (2021). Mechanisms underlying pre- and postnatal
898 development of the vomeronasal organ. Cell Mol Life Sci.
899 Katreddi, R.R., Taroc, E.Z.M., Hicks, S.M., Lin, J.M., Liu, S., Xiang, M., and Forni, P.E.
900 (2021). Notch signaling determines cell-fate specification of the two main types of
901 vomeronasal neurons of rodents. bioRxiv, 2021.2010.2026.466003.
902 Keller, M., Pierman, S., Douhard, Q., Baum, M.J., and Bakker, J. (2006). The
903 vomeronasal organ is required for the expression of lordosis behaviour, but not sex
904 discrimination in female mice. The European journal of neuroscience *23*, 521-530.
905 Koolhaas, J.M., Coppens, C.M., de Boer, S.F., Buwalda, B., Meerlo, P., and
906 Timmermans, P.J.A. (2013). The resident-intruder paradigm: a standardized test for
907 aggression, violence and social stress. Journal of visualized experiments : JoVE, e4367-
908 e4367.
909 Krieger, J., Schmitt, A., Lobel, D., Gudermann, T., Schultz, G., Breer, H., and Boekhoff,
910 I. (1999). Selective activation of G protein subtypes in the vomeronasal organ upon
911 stimulation with urine-derived compounds. The Journal of biological chemistry *274*, 4655-
912 4662.
913 Langmead, B., and Salzberg, S.L. (2012). Fast gapped-read alignment with Bowtie 2.
914 Nature methods *9*, 357-359.
915 Lin, J.M., Taroc, E.Z.M., Frias, J.A., Prasad, A., Catizone, A.N., Sammons, M.A., and
916 Forni, P.E. (2018). The transcription factor Tfap2e/AP-2epsilon plays a pivotal role in
917 maintaining the identity of basal vomeronasal sensory neurons. Dev Biol *441*, 67-82.
918 Luo, L., Ambrozkiewicz, M.C., Benseler, F., Chen, C., Dumontier, E., Falkner, S.,
919 Furlanis, E., Gomez, A.M., Hoshina, N., Huang, W.H.*, et al.* (2020). Optimizing Nervous
920 System-Specific Gene Targeting with Cre Driver Lines: Prevalence of Germline
921 Recombination and Influencing Factors. Neuron *106*, 37-65 e35.
922 Lupien, M., Eeckhoute, J., Meyer, C.A., Wang, Q., Zhang, Y., Li, W., Carroll, J.S., Liu,
923 X.S., and Brown, M. (2008). FoxA1 translates epigenetic signatures into enhancer-driven
924 lineage-specific transcription. Cell *132*, 958-970.
925 Magnani, L., Eeckhoute, J., and Lupien, M. (2011). Pioneer factors: directing
926 transcriptional regulators within the chromatin environment. Trends Genet *27*, 465-474.
927 Mangale, V.S., Hirokawa, K.E., Satyaki, P.R., Gokulchandran, N., Chikbire, S.,
928 Subramanian, L., Shetty, A.S., Martynoga, B., Paul, J., Mai, M.V.*, et al.* (2008). Lhx2
929 selector activity specifies cortical identity and suppresses hippocampal organizer fate.
930 Science *319*, 304-309.

931 Martin, M. (2011). Cutadapt removes adapter sequences from high-throughput
932 sequencing reads. EMBnetjournal *17*, 10-12.
933 Martinez-Marcos, A., Ubeda-Banon, I., and Halpern, M. (2000). Cell turnover in the
934 vomeronasal epithelium: evidence for differential migration and maturation of subclasses
935 of vomeronasal neurons in the adult opossum. Journal of neurobiology *43*, 50-63.
936 Matsunami, H., and Buck, L.B. (1997). A multigene family encoding a diverse array of
937 putative pheromone receptors in mammals. Cell *90*, 775-784.
938 Meers, M.P., Bryson, T.D., Henikoff, J.G., and Henikoff, S. (2019). Improved CUT&RUN
939 chromatin profiling tools. Elife *8*.
940 Mohrhardt, J., Nagel, M., Fleck, D., Ben-Shaul, Y., and Spehr, M. (2018). Signal Detection
941 and Coding in the Accessory Olfactory System. Chemical senses *43*, 667-695.
942 Molyneaux, B.J., Arlotta, P., Menezes, J.R., and Macklis, J.D. (2007). Neuronal subtype
943 specification in the cerebral cortex. Nature reviews Neuroscience *8*, 427-437.
944 Mombaerts, P., Wang, F., Dulac, C., Chao, S.K., Nemes, A., Mendelsohn, M.,
945 Edmondson, J., and Axel, R. (1996). Visualizing an olfactory sensory map. Cell *87*, 675-
946 686.
947 Monahan, K., Schieren, I., Cheung, J., Mumbey-Wafula, A., Monuki, E.S., and
948 Lomvardas, S. (2017). Cooperative interactions enable singular olfactory receptor
949 expression in mouse olfactory neurons. eLife *6*.
950 Montani, G., Tonelli, S., Sanghez, V., Ferrari, P.F., Palanza, P., Zimmer, A., and Tirindelli,
951 R. (2013). Aggressive behaviour and physiological responses to pheromones are strongly
952 impaired in mice deficient for the olfactory G-protein -subunit G8. J Physiol *591*, 3949-
953 3962.
954 Murray, R.C., Navi, D., Fesenko, J., Lander, A.D., and Calof, A.L. (2003). Widespread
955 defects in the primary olfactory pathway caused by loss of Mash1 function. The Journal
956 of neuroscience : the official journal of the Society for Neuroscience *23*, 1769-1780.
957 Naik, A.S., Lin, J.M., Taroc, E.Z.M., Katreddi, R.R., Frias, J.A., Lemus, A.A., Sammons,
958 M.A., and Forni, P.E. (2020). Smad4-dependent morphogenic signals control the
959 maturation and axonal targeting of basal vomeronasal sensory neurons to the accessory
960 olfactory bulb. Development *147*, dev184036.
961 Norlin, E.M., Alenius, M., Gussing, F., Hagglund, M., Vedin, V., and Bohm, S. (2001).
962 Evidence for gradients of gene expression correlating with zonal topography of the
963 olfactory sensory map. Mol Cell Neurosci *18*, 283-295.
964 Oboti, L., Ibarra-Soria, X., Perez-Gomez, A., Schmid, A., Pyrski, M., Paschek, N., Kircher,
965 S., Logan, D.W., Leinders-Zufall, T., Zufall, F.*, et al.* (2015). Pregnancy and estrogen
966 enhance neural progenitor-cell proliferation in the vomeronasal sensory epithelium. BMC
967 Biol *13*, 104.
968 Oboti, L., Perez-Gomez, A., Keller, M., Jacobi, E., Birnbaumer, L., Leinders-Zufall, T.,
969 Zufall, F., and Chamero, P. (2014). A wide range of pheromone-stimulated sexual and
970 reproductive behaviors in female mice depend on G protein Galphao. BMC Biol *12*, 31.
971 Pankevich, D.E., Baum, M.J., and Cherry, J.A. (2004). Olfactory sex discrimination
972 persists, whereas the preference for urinary odorants from estrous females disappears in
973 male mice after vomeronasal organ removal. The Journal of neuroscience : the official
974 journal of the Society for Neuroscience *24*, 9451-9457.
975 Patel, T., and Hobert, O. (2017). Coordinated control of terminal differentiation and
976 restriction of cellular plasticity. eLife *6*.

977 Patel, T., Tursun, B., Rahe, D.P., and Hobert, O. (2012). Removal of Polycomb repressive
978 complex 2 makes C. elegans germ cells susceptible to direct conversion into specific
979 somatic cell types. Cell reports *2*, 1178-1186.
980 Pellikainen, J.M., and Kosma, V.M. (2007). Activator protein-2 in carcinogenesis with a
981 special reference to breast cancer--a mini review. International journal of cancer Journal
982 international du cancer *120*, 2061-2067.
983 Pereira, L., Aeschimann, F., Wang, C., Lawson, H., Serrano-Saiz, E., Portman, D.S.,
984 Grosshans, H., and Hobert, O. (2019). Timing mechanism of sexually dimorphic nervous
985 system differentiation. eLife *8*.
986 Perez-Gomez, A., Stein, B., Leinders-Zufall, T., and Chamero, P. (2014). Signaling
987 mechanisms and behavioral function of the mouse basal vomeronasal neuroepithelium.
988 Frontiers in neuroanatomy *8*, 135.
989 Polanco, J., Reyes-Vigil, F., Weisberg, S.D., Dhimitruka, I., and Bruses, J.L. (2021).
990 Differential Spatiotemporal Expression of Type I and Type II Cadherins Associated With
991 the Segmentation of the Central Nervous System and Formation of Brain Nuclei in the
992 Developing Mouse. Front Mol Neurosci *14*, 633719.
993 Prince, J.E., Brignall, A.C., Cutforth, T., Shen, K., and Cloutier, J.F. (2013). Kirrel3 is
994 required for the coalescence of vomeronasal sensory neuron axons into glomeruli and for
995 male-male aggression. Development *140*, 2398-2408.
996 Prince, J.E., Cho, J.H., Dumontier, E., Andrews, W., Cutforth, T., Tessier-Lavigne, M.,
997 Parnavelas, J., and Cloutier, J.F. (2009). Robo-2 controls the segregation of a portion of
998 basal vomeronasal sensory neuron axons to the posterior region of the accessory
999 olfactory bulb. The Journal of neuroscience : the official journal of the Society for
1000 Neuroscience *29*, 14211-14222.
1001 Rahe, D.P., and Hobert, O. (2019). Restriction of Cellular Plasticity of Differentiated Cells
1002 Mediated by Chromatin Modifiers, Transcription Factors and Protein Kinases. G3
1003 (Bethesda) *9*, 2287-2302.
1004 Rothstein, M., and Simoes-Costa, M. (2020). Heterodimerization of TFAP2 pioneer
1005 factors drives epigenomic remodeling during neural crest specification. Genome Res *30*,
1006 35-48.
1007 Ryba, N.J., and Tirindelli, R. (1997). A new multigene family of putative pheromone
1008 receptors. Neuron *19*, 371-379.
1009 Seberg, H.E., Van Otterloo, E., Loftus, S.K., Liu, H., Bonde, G., Sompallae, R., Gildea,
1010 D.E., Santana, J.F., Manak, J.R., Pavan, W.J.*, et al.* (2017). TFAP2 paralogs regulate
1011 melanocyte differentiation in parallel with MITF. PLoS Genet *13*, e1006636.
1012 Silva, L., and Antunes, A. (2017). Vomeronasal Receptors in Vertebrates and the
1013 Evolution of Pheromone Detection. Annu Rev Anim Biosci *5*, 353-370.
1014 Silvotti, L., Cavaliere, R.M., Belletti, S., and Tirindelli, R. (2018). In-vivo activation of
1015 vomeronasal neurons shows adaptive responses to pheromonal stimuli. Scientific reports
1016 *8*, 8490.
1017 Skene, P.J., Henikoff, J.G., and Henikoff, S. (2018). Targeted in situ genome-wide
1018 profiling with high efficiency for low cell numbers. Nature protocols *13*, 1006-1019.
1019 Skene, P.J., and Henikoff, S. (2017). An efficient targeted nuclease strategy for high-
1020 resolution mapping of DNA binding sites. eLife *6*.
1021 Stefanakis, N., Carrera, I., and Hobert, O. (2015). Regulatory Logic of Pan-Neuronal
1022 Gene Expression in C. elegans. Neuron *87*, 733-750.

1023 Stowers, L., Holy, T.E., Meister, M., Dulac, C., and Koentges, G. (2002). Loss of sex
1024 discrimination and male-male aggression in mice deficient for TRP2. Science *295*, 1493-
1025 1500.
1026 Taroc, E.Z.M., Naik, A.S., Lin, J.M., Peterson, N.B., Keefe, D.L., Jr., Genis, E., Fuchs, G.,
1027 Balasubramanian, R., and Forni, P.E. (2020). Gli3 Regulates Vomeronasal
1028 Neurogenesis, Olfactory Ensheathing Cell Formation, and GnRH-1 Neuronal Migration.
1029 The Journal of neuroscience : the official journal of the Society for Neuroscience *40*, 311-
1030 326.
1031 Trouillet, A.C., Keller, M., Weiss, J., Leinders-Zufall, T., Birnbaumer, L., Zufall, F., and
1032 Chamero, P. (2019). Central role of G protein Galphai2 and Galphai2(+) vomeronasal
1033 neurons in balancing territorial and infant-directed aggression of male mice. Proc Natl
1034 Acad Sci U S A *116*, 5135-5143.
1035 Trouillet, A.C., Moussu, C., Poissenot, K., Keller, M., Birnbaumer, L., Leinders-Zufall, T.,
1036 Zufall, F., and Chamero, P. (2021). Sensory Detection by the Vomeronasal Organ
1037 Modulates Experience-Dependent Social Behaviors in Female Mice. Front Cell Neurosci
1038 *15*, 638800.
1039 Vaddadi, N., Iversen, K., Raja, R., Phen, A., Brignall, A., Dumontier, E., and Cloutier, J.F.
1040 (2019). Kirrel2 is differentially required in populations of olfactory sensory neurons for the
1041 targeting of axons in the olfactory bulb. Development *146*.
1042 Walz, A., Rodriguez, I., and Mombaerts, P. (2002). Aberrant sensory innervation of the
1043 olfactory bulb in neuropilin-2 mutant mice. The Journal of neuroscience : the official
1044 journal of the Society for Neuroscience *22*, 4025-4035.
1045 Wankhade, S., Yu, Y., Weinberg, J., Tainsky, M.A., and Kannan, P. (2000).
1046 Characterization of the activation domains of AP-2 family transcription factors. The
1047 Journal of biological chemistry *275*, 29701-29708.
1048 Weiler, E., McCulloch, M.A., and Farbman, A.I. (1999). Proliferation in the vomeronasal
1049 organ of the rat during postnatal development. The European journal of neuroscience *11*,
1050 700-711.
1051 Williams, C.M., Scibetta, A.G., Friedrich, J.K., Canosa, M., Berlato, C., Moss, C.H., and
1052 Hurst, H.C. (2009). AP-2gamma promotes proliferation in breast tumour cells by direct
1053 repression of the CDKN1A gene. EMBO J *28*, 3591-3601.
1054 Wilson, K.C.P., and Raisman, G. (1980). Age-related changes in the neurosensory
1055 epithelium of the mouse vomeronasal organ: Extended period of post-natal growth in size
1056 and evidence for rapid cell turnover in the adult. Brain research *185*, 103-113.
1057 Yu, G., Wang, L.G., Han, Y., and He, Q.Y. (2012). clusterProfiler: an R package for
1058 comparing biological themes among gene clusters. OMICS *16*, 284-287.
1059 Yu, G., Wang, L.G., and He, Q.Y. (2015). ChIPseeker: an R/Bioconductor package for
1060 ChIP peak annotation, comparison and visualization. Bioinformatics *31*, 2382-2383.
1061 Zhang, Y., Liu, T., Meyer, C.A., Eeckhoute, J., Johnson, D.S., Bernstein, B.E., Nusbaum,
1062 C., Myers, R.M., Brown, M., Li, W.*, et al.* (2008). Model-based analysis of ChIP-Seq
1063 (MACS). Genome biology *9*, R137.
1064 Zuloaga, D.G., Morris, J.A., Monks, D.A., Breedlove, S.M., and Jordan, C.L. (2007).
1065 Androgen-sensitivity of somata and dendrites of spinal nucleus of the bulbocavernosus
1066 (SNB) motoneurons in male C57BL6J mice. Hormones and behavior *51*, 207-212.
1067

1068 **FIGURE LEGENDS**

1069
1070 **Figure 1: Analysis of single cell sequencing data of the vomeronasal organ.** P10
1071 male controls shows the developing vomeronasal neurons as they progress through A-
1072 C) neurogenesis (Ascl1, Neurog1, Neurod1), D-E) maturation (Gap43, OMP), and F-I)
1073 apical and basal differentiation (Bcl11b, Tfap2e, Meis2). A) Ascl1 is expressed by
1074 transiently amplifying progenitor cells (cyan arrow), which transition into the immediate
1075 neuronal precursors that turn on pro-neural genes (cyan arrow) Neurog1 (B) and Neurod1
1076 (C) and turn off as the precursors turn into immature neurons (black and magenta). D)
1077 Immature neurons express Gap43, which persists in both apical (black arrow) and basal
1078 (magenta arrow) branches, until it declines as neurons begin to reach maturity and
1079 express E) OMP in mature apical (black arrow) and mature basal (magenta arrow) VSNs.
1080 Gap43 and OMP expression briefly overlap, as the neurons transition to a fully
1081 differentiated mature stage. F) Bcl11b mRNA expression is found in both apical and basal
1082 VSNs but at different developmental timepoints. Bcl11b is found in committed basal
1083 precursors near the establishment of the apical/basal dichotomy (magenta arrow) but is
1084 not found until later in apical VSN development (black arrow) G) AP-2ε is expressed by
1085 the basal branch (magenta arrows) and H) Meis2 mRNA expression is found in the apical
1086 branch (black arrows) and even in early neurogenesis stages (cyan arrow), and their
1087 expression does not overlap. J) Enhanced volcano plot. Differential gene expression
1088 between apical and basal branches of VSNs. Apical specific genes (55 genes) trend left
1089 and basal specific genes (187 genes) trend right. Significance defined as Log_2-Fold
1090 Change > 0.3 and Adjusted p-value ≤ 0.05.
1091
1092
1093
1094 **<u>Figure 2:</u> KO mouse generation and characterization of rescued AP2e expression.**
1095 A) Knock-in strategy through homologous recombination to generate the R26AP2ε mouse
1096 line. The CAG-loxP-stop-loxP-mouse-Tfap2e cassette as integrated into the first intron of
1097 Rosa26 B-C) Immunohistochemistry on P21 wild-type (B, E, H), AP-2εNull (C, F, I), and
1098 AP-$2\varepsilon^{Rescue}$ (D, G, J) mice against AP-2ε and Cre recombinase. B-B') In WT mice AP-2ε
1099 expression is in the marginal zones (MZ) and in the basal regions of the VSNs. C) In AP-
1100 $2\varepsilon^{Null}$ mice, no AP-2ε immunoreactivity is observed but lost in the central regions where
1101 more mature neurons reside. D) In the AP-$2\varepsilon^{Rescue}$, AP-2ε expression in the basal region,
1102 but with less intensity and density at the tips compared to WT controls. E-G)
1103 Immunostainings against V2R2 (magenta) and Meis2 (green) counterstained with DAPI
1104 (white). H-J) Immunostainings against Gαo (magenta) and Gαi2 (green) counterstained
1105 with DAPI). K) AP-2εNull mice show a dramatic reduction in basal VSNs and apical VSNs
1106 occupy most of the epithelium (E, F, H, I, K). D, G, J, K) The AP-$2\varepsilon^{Rescue}$ has an
1107 intermediate phenotype between WT and AP-$2\varepsilon^{Null}$ mice, where the VNE contains more
1108 basal VSNs than in the AP-$2\varepsilon^{Null}$ mice but does not reach the equivalency of the WT (K).
1109
1110
1111 **<u>Figure 3:</u> Territorial aggression and sex preference depends on AP-2ε expression**
1112 **in mice.** A) The odorant preference paradigm where cotton swabs with either male or
1113 female whole urine are placed on opposite ends of a test cage and the amount of time
1114 spent smelling each odorant is measured. B) Male wild-type mice spent significantly more

time investigating female odorants than male odorants. Preference for female odorants is lost in AP-2ε KO male mice but restored in AP-2ε rescue mice. C) Male-male aggression was evaluated using the Resident intruder paradigm B) Wild-type mice display aggressive behaviors toward male intruders and number of attacks were quantified. C) AP-2ε Null mice attacked intruders significantly less than WT mice. However, AP-2ε Rescue mice showed significantly more aggressive behaviors that is not significantly different than the WT male mice. G) Seminal vesicle weight was not significantly different across all genotypes when normalized to bodyweight.

<u>Figure 4</u>: Ectopic expression of AP-2ε in the MOE and the VNE promotes expression of basal markers. Immunostainings at P10 on OMPCre$^{+/-}$ controls (A-D) and OMPCre$^{+/-}$/R26AP2ε$^{+/-}$ mutants (E-H). A) IHC against AP-2ε in the VNOs of shows that AP-2ε is expressed in only the basal VSNs (arrow) in Controls but have extended AP-2ε immunoreactivity into apical (magenta arrowheads) and sustentacular regions (white arrowheads) in the Ectopic mutant. B,F) ISH against Gαo show that in controls (B) Gαo mRNA expression is restricted to the basal regions of the VNE. F) Ectopic AP-2ε mutants show Gαo mRNA reactivity in the apical regions of the VNE (magenta arrowheads). C,G) Immunohistochemistry against V2R2 in the VNO of controls (C) shows no immunoreactivity in the apical regions of the VNE in controls (notched arrows) and is limited to the basal VSNs (black arrow). G) In mutants, more of the vomeronasal epithelium was positive for V2R2 in mutants, as expression expands into the apical regions of the epithelium (magenta arrowheads). D-H') P10 VNOs immunostained against Gαo (green) and V2R2 (magenta) show that Gαo and V2R2 colocalize almost completely in the basal regions of the VNE. OMPCre$^{+/-}$/R26AP2ε$^{+/-}$ mutants have Gαo/V2R2 positive VSNs localized in apical regions of the VNE. I-J) Violin plot of Gαo (I), and Vmn2r7 (J) mRNA expression between apical and basal VSNs in OMPCre$^{+/-}$ controls and apical VSNs of OMPCre$^{+/-}$/R26AP2ε$^{+/-}$ mutant mice show significant upregulation of basal markers based on p.value ($p<0.05$ = *, $p<0.0004$ = ****). K,L) Quantifications at P10 show a significant increase in the amount of the neuroepithelium positive for V2R2 (I) and Gαo (J). Quantifications at P21 show significantly more of the epithelium is V2R2+. (K) The amount of the epithelium positive for Gαo is not significantly different between genotypes (L). M, O) Immunofluorescence against V2R2 (magenta) and Meis2 (green) in controls (M) and OMPCre$^{+/-}$/R26AP2ε$^{+/-}$ mutants (O). N, P) Immunofluorescence against Gαo (magenta) in control (N) and OMPCre$^{+/-}$/R26AP2ε$^{+/-}$ mutant (P). Q) Our quantifications show that ectopic mutants have significantly more cells positive for basal markers in the apical regions than controls.

<u>Figure 5:</u> Progressive changes in VNE lamination may reflect the changing expression profiles of cell adhesion molecules in apical VSNs. Immunofluorescence against Sox2 (cyan), AP-2ε (magenta), and Meis2 (green) with DAPI (blue) counterstain. Neuroepithelium traced in yellow dotted line. A) P21 WT Controls show highly organized stratified neuroepithelium with contiguous layers of AP-2ε+/basal (magenta), Meis2+/apical (green), and Sox2+/sustentacular cell (cyan) layers. B-C) OMPCre$^{+/-}$/R26AP2ε$^{+/-}$ VNO at B) P21 show that Sox2+/sustentacular cells have intraepithelial cysts

with internalized subsidiary lumens (red arrows) C) In adults (3mo) OMPCre$^{+/-}$/R26AP2ε$^{+/-}$ mutants show an increase in the severity of intraepithelial cysts (red arrows) and breaks in the sustentacular layer and expansion of neurons to the luminal surface (red notched arrows). Unidentified matter (*) reactive to anti-mouse Abs was detected within the cysts. D) Quantifications of the zonal distribution through Zone 1 (dorsal) -> Zone 7 (ventral) of these cytoarchitecture abnormalities (which include both cell body abnormalities and dendritic disorganization, each point = 1 animal) show that these disruptions occur in the intermediate and central regions of the VNO, but not in the marginal zones (MZ, Zone1,7). The highest rate of occurrence are in zone 3 and 6, which are intermediate regions in the VNO. E) Dot plot showing that composition and intensity of differentially expressed genes involved in cellular adhesion in the VSNs of controls and ectopic AP-2ε mutants.

<u>Figure 6:</u> Single-cell sequencing of P10 OMPCre$^{+/-}$ control and OMPCre$^{+/-}$R26AP2ε$^{+/-}$ mutant VSNs indicate a shift in apical cells towards basal cells in the mutant. A-A'''') UMAP clustering of VSNs from progenitor cells to differentiated mature apical and basal cells of Control B-B''') Mutant mice split by genotype. A'-A''', B'-B''') Blended feature plots of AP-2ε expression (red) and Meis2 (blue). Red arrowheads indicate onset of AP-2ε expression. Black arrow indicates mature apical VSNs. OMPCre$^{+/-}$ Controls (A'-A''') show a divergent pattern of expression where the onset of AP-2ε (red, red arrowhead) is only on the basal branch. Meis2 expression (blue) occurs only on the apical branch where the cells lack AP-2ε expression. OMPCre$^{+/-}$R26AP2e$^{+/-}$ mutants (B'-B''') start to express AP-2ε on the basal branch in immature basal VSNs, however, onset of AP-2ε mRNA expression also occurs on the apical branch where OMP expression begins (red arrowhead). AP-2ε mRNA is co-expressed with Meis2 mRNA in in apical VSNs from ectopic mutants (red arrowhead arrow). We found that these cells clustered separately from mature apical cells from the control and mature basal cells from the mutant but are a unique population that bridge the gap between normal apical and basal cells (arrows). D) Violin plot shows Calreticulin (Calr) mRNA expression levels in apical VSNs from the OMPCre$^{+/-}$R26AP2ε$^{+/-}$ mutants are reduced to levels similar to basal VSNs from OMPCre$^{+/-}$ controls. E) Violin plot shows Calreticulin-4 (Calr4) mRNA expression levels. E) In control cells, AP-2ε mRNA expression (red arrowheads) and Meis2 mRNA expression (blue) are not co-expressed in the same cells. AP-2ε expression is upregulated in immature basal VSNs and not apical VSNs. F-G) ISH against Calr4 against P11 OMPCre$^{+/-}$ controls(G) and OMPCre$^{+/-}$R26AP2ε$^{+/-}$ mutants (G) show that while Calr4 mRNA is normally enriched in basal VSNs (arrowheads), ectopic AP-2ε mutants show expansion of Calr4 positivity in the apical regions when compared to controls (arrows). H-K) Analysis of CUT&RUN against Tfap2e/AP-2ε. H) Tornado plot of AP-2ε occupancy in the dissociated tissue of the VNO. The genomic regions are defined as the summit +/- 1kb. I) Pie chart depicting the genomic distribution of putative AP-2ε binding sites show that most of AP-2ε peaks are found in promoter regions of putative target genes and to a lesser extent in intergenic and intronic regions of the genome. J) Venn diagram of the determined AP-2ε targets and the genes enriched in the basal and apical VSNs. K) Venn diagram of the determined AP-2ε targets and all the upregulated and downregulated genes in the ectopic AP-2ε mutant mouse. Significance defined by Adjusted p-value ≤ 0.05.

1205
1206 **<u>Figure 7:</u> Ectopic AP-2ε expression alters the detection of sex-specific odorants**. A-
1207 D) Immunofluorescence against pS6 (magenta, arrows) and Meis2 (green) with DAPI
1208 counterstain (blue) in the VNE of Controls (A,C) and OMPCreR26AP-2ε mutants (B,D).
1209 A-B) VNE of adult male wildtype and ectopic mutants when exposed to male soiled
1210 bedding show similar activation or pS6 immunoreactivity (arrows) in Meis2+/apical and
1211 Meis2-/basal VSNs. C,D) VNE of adult female wildtype and ectopic mutants when
1212 exposed to female soiled bedding show the while WT females displayed a higher
1213 proportion of pS6+ apical VSNs OMPCre$^{+/-}$/R26AP-2ε$^{+/-}$ mutants showed a decreased
1214 number of activated Meis2+/apical VSNs. In both exposure conditions ectopic activation
1215 of sustentacular cells (notched arrows) and VSNs near the lumen (arrowheads). E)
1216 Quantifications of activated VSNs in male mice after exposure to male-soiled bedding
1217 show similar activation between mutants and controls. Small but non-significant increase
1218 in the total number of activated basal VSNs. F) Quantifications of activated VSNs after
1219 exposure to sex-specific odorants in female mice show a significant decrease in the
1220 number of activated apical VSNs with no change in the number of activated VSNs
1221 between female OMPCre$^{+/-}$/R26AP-2ε$^{+/-}$ mutants and controls. G) Quantifications of the
1222 number of attacks for all WT and OMPCre$^{+/-}$/R26AP-2ε$^{+/-}$ mutants in a resident intruder
1223 test show male ectopic AP-2ε mice display higher levels of intermale aggression, but are
1224 not significantly different than controls. H) Quantifications of odorant preference tests in
1225 male and female mice show that male and female OMPCre$^{+/-}$/R26AP-2ε$^{+/-}$ mutants retain
1226 the preference for opposite sex odorants. Significance defined as p-value ≤ 0.05.
1227

1228 **SUPPLEMENTARY FIGURE LEGENDS**
1229
1230 **<u>Supplementary Figure S1</u>: Expression of potential AP-2 co-factors in both apical**
1231 **and basal VSNs.** Featureplots of known AP-2 family cofactors p300/CBP, Cited2, Cited4,
1232 Kctd1, Sp1, Sp8, Yy1 in P10 VSNs.
1233
1234 **<u>Supplementary Figure S2</u>: AP-2ε and V2R2 immunoreactivity in the MOE.** P10
1235 OMPCre$^{+/-}$ controls(A,C) and OMPCre$^{+/-}$/R26AP-2ε$^{+/-}$ ectopic mutants (B,D). A-B)
1236 Immunohistochemistry against AP-2ε in the main olfactory epithelium (OE) shows no
1237 immunoreactivity in controls (black notched arrows) and ectopic AP-2ε expression in the
1238 mutants (magenta arrowheads). C-D) Immunohistochemistry against V2R2 in the main
1239 olfactory epithelium (OE) shows no expression in either control (C) nor ectopic AP-2ε
1240 mutant (D).
1241
1242 **<u>Supplementary Figure S3:</u> Analysis of Sustentacular Cells**. A-F)
1243 Immunofluorescence on Wildtype (A-C) and OMPCre$^{+/-}$/R26AP2ε$^{+/-}$ mutants (D-F) against
1244 AP-2ε (magenta) and Sox2 (green) counterstained with DAPI (blue). A-C) A-C) WT
1245 controls and ectopic AP-2ε mutants (D-F) show sustentacular (sus) cells with high
1246 immunoreactivity for Sox2 and no AP-2ε expression. Apical (a) VSNs closest to the
1247 sustentacular cell layer show low immunoreactivity for Sox2 (brackets, arrowheads) with
1248 apical VSNs closer to basal (b) VSNs with no immunodetectable Sox2 (notched arrows).
1249 no colocalization between AP-2ε and Sox2+ sustentacular cells (sus). D-F) OMPCre$^{+/-}$
1250 /R26AP2ε$^{+/-}$ mice have some Sox2+ sustentacular cells that have ectopic AP-2ε
1251 expression (arrows). G) UMAPs of sustentacular cells from OMPCre$^{+/-}$/R26AP2ε$^{+/-}$ adults
1252 showed that AP2ε positive and negative clusters segregated from each other with
1253 accompanying feature plots showing the expression of sustentacular cell markers Hes1,
1254 Krt8, and Cyp2a5 along with ectopic Tfap2e/AP-2ε mRNA expression. H) Gene ontology
1255 analysis of Tfap2e+ sustentacular cells showed an enrichment of dysregulated genes
1256 related to cytoskeleton organization, cell-cell junction organization, cytoskeletal
1257 organization, and cytoplasmic ribosomal proteins. I) Heatmap of up- and down-regulated
1258 genes found related to cytoskeleton organization, cell-cell junction organization, and
1259 cytoskeleton organization in Tfap2e positive and negative sustentacular cells.
1260
1261 **<u>Supplementary Figure S4:</u> Analysis of the AOBs from adult WT and OMPCre$^{+/-}$**
1262 **/R26AP2ε$^{+/-}$ mice.** A-B) Immunofluorescence against Nrp2 (green) and Robo2 (red) and
1263 counterstained with DAPI (blue) showed that the expression of guidance cue molecules
1264 in WT (A) and OMPCre$^{+/-}$/R26AP2ε$^{+/-}$ (B) mice was comparable and showed distinct
1265 anterior and posterior AOB regions (arrows). C,D) Immunofluorescence against Kirrel2
1266 (green) and Kirrel3 (red) and DAPI (blue) counterstain on WT (C) and OMPCre$^{+/-}$
1267 /R26AP2ε$^{+/-}$ (D) AOBs showed the glomerular organization and morphology was
1268 comparable between genotypes (arrows). Similar E) Quantifications of the average area
1269 of the AOB was not significantly different across genotypes. Analysis of the glomeruli size
1270 (F) and number (G) using IF against Kirrel2 and Kirrel3 showed no significant changes
1271 across genotypes.
1272

1273 **Supplementary Figure S5:** A) AP-2ε binding in WT and OMPCreR26AP2ε mutants at
1274 TSS of apical and basal enriched genes and the significantly up- and down-regulated
1275 genes in the OMPCreR26AP2ε mutants. B) AP-2ε enrichment at putative activated and
1276 repressed target genes in the OMPCreR26AP2ε ectopic mutant shows greater
1277 enrichment at up-regulated targets. C) Dot plot of enriched GO terms show many putative
1278 AP-2ε target genes being chromatin or histone modifiers. D) Motif enrichment analysis
1279 validated our analysis as Tfap2 was the top motif found at putative binding sites. It also
1280 yielded TF family motifs of potential cofactors including SP, KLF, EBF, RFX, ELK, NRF,
1281 DLX, and LHX transcription factor families. E) Tracks from CUT&RUN sequencing where
1282 AP-2ε peaks are found in the promoter regions of activated (purple) and repressed
1283 (yellow) genes.
1284
1285 **Supplementary Figure S6: Differential gene expression analysis from scSeq in**
1286 **adult animals of apical and basal populations scSeq in Adults WT Controls and**
1287 **OMPCre$^{+/-}$/R26AP2ε$^{+/-}$ VNOs.** A) Volcano Plot of significantly up- and down-regulated
1288 genes in apical VSNs in adult WT and OMPCre$^{+/-}$/R26AP2ε$^{+/-}$ mice show dysregulation of
1289 many key basal genes and down-regulation of apical-enriched genes. B) Volcano Plot of
1290 significantly up and downregulated genes in basal VSNs in adult WT and OMPCre$^{+/-}$
1291 /R26AP2ε$^{+/-}$ mice show that some genes may respond to AP-2ε regulation in a dose-
1292 dependent manner. C) Dot plot of canonical genes expressed by apical and basal VSNs
1293 and key genes identified in scSeq analysis for P10 and Adult Control and Mutant mice.
1294
1295
1296
1297

1298 **SUPPLEMENTARY TABLES**
1299
1300 **Supplementary Table S1:**
1301 **Genes enriched in apical and basal populations of VSNs**
1302 Significance defined as Adjusted p-value ≤ 0.05
1303
1304
1305
1306
1307 **Supplementary Table S2:**
1308 **Significantly dysregulated genes in apical VSNs from OMPCreR26AP2ε mice**
1309 Significance defined as Adjusted p-value ≤ 0.05
1310
1311

1312 **GRAPHICAL ABSTRACT**

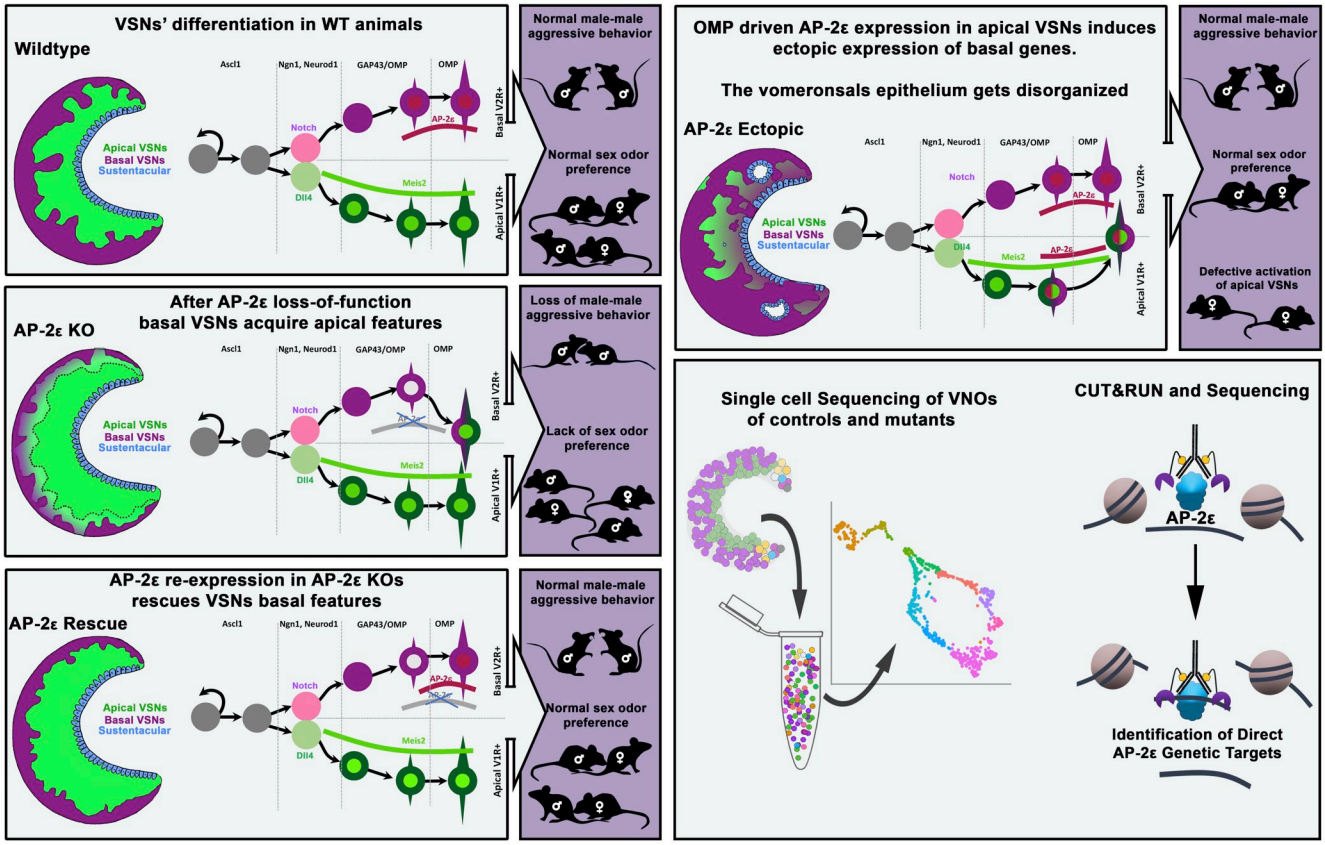

1313
1314
1315
1316
1317
1318
1319
1320
1321
1322
1323

FIGURE 1

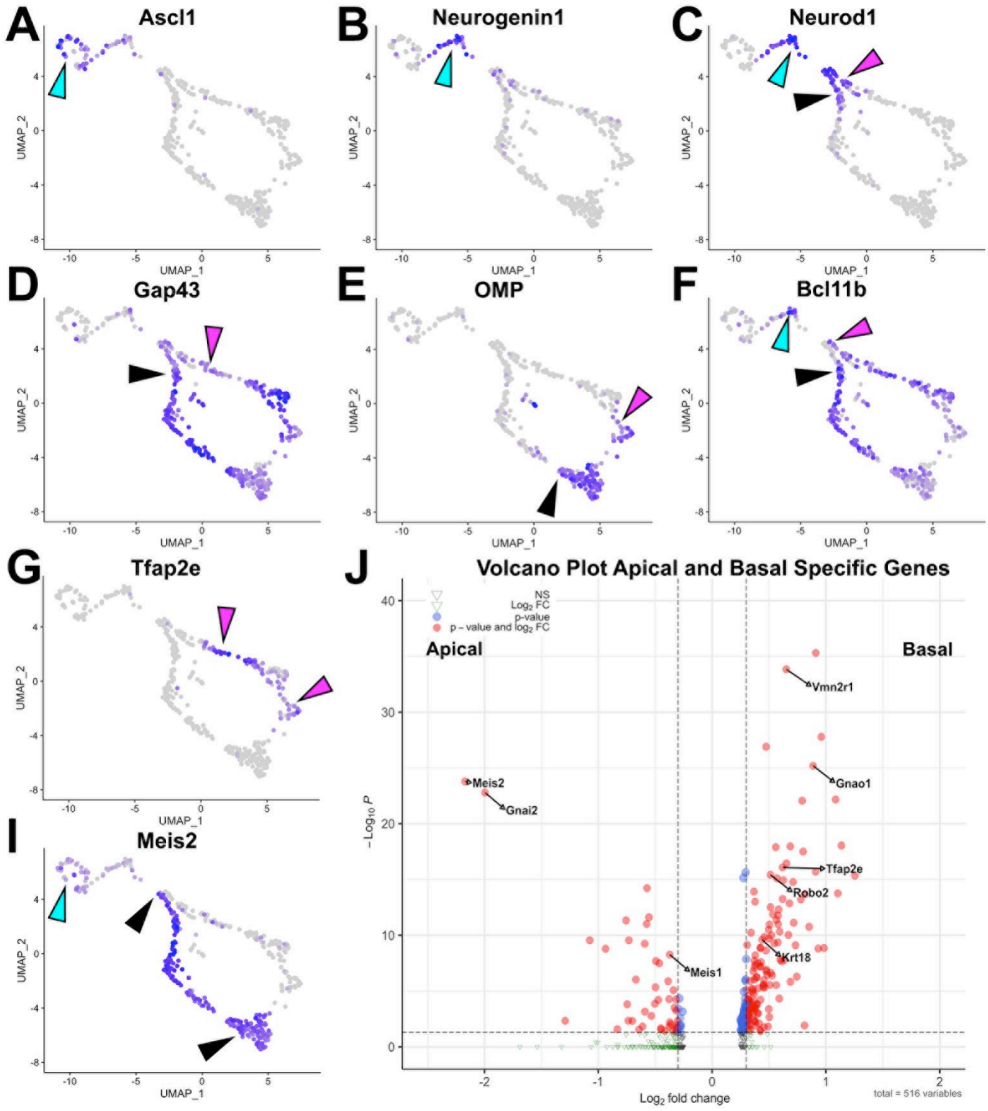
A
Ascl1
B
Neurogenin1
C
Neurod1
D
Gap43
E
OMP
F
Bcl11b
G
Tfap2e
I
Meis2
J
Volcano Plot Apical and Basal Specific Genes
NS
Log2 FC
p-value
p – value and log2 FC
Apical
Basal
Vmn2r1
Gnao1
Meis2
Gnai2
Tfap2e
Robo2
Krt18
Meis1
−Log10 P
Log2 fold change
total = 516 variables
UMAP_1
UMAP_2

1331 **FIGURE 2**

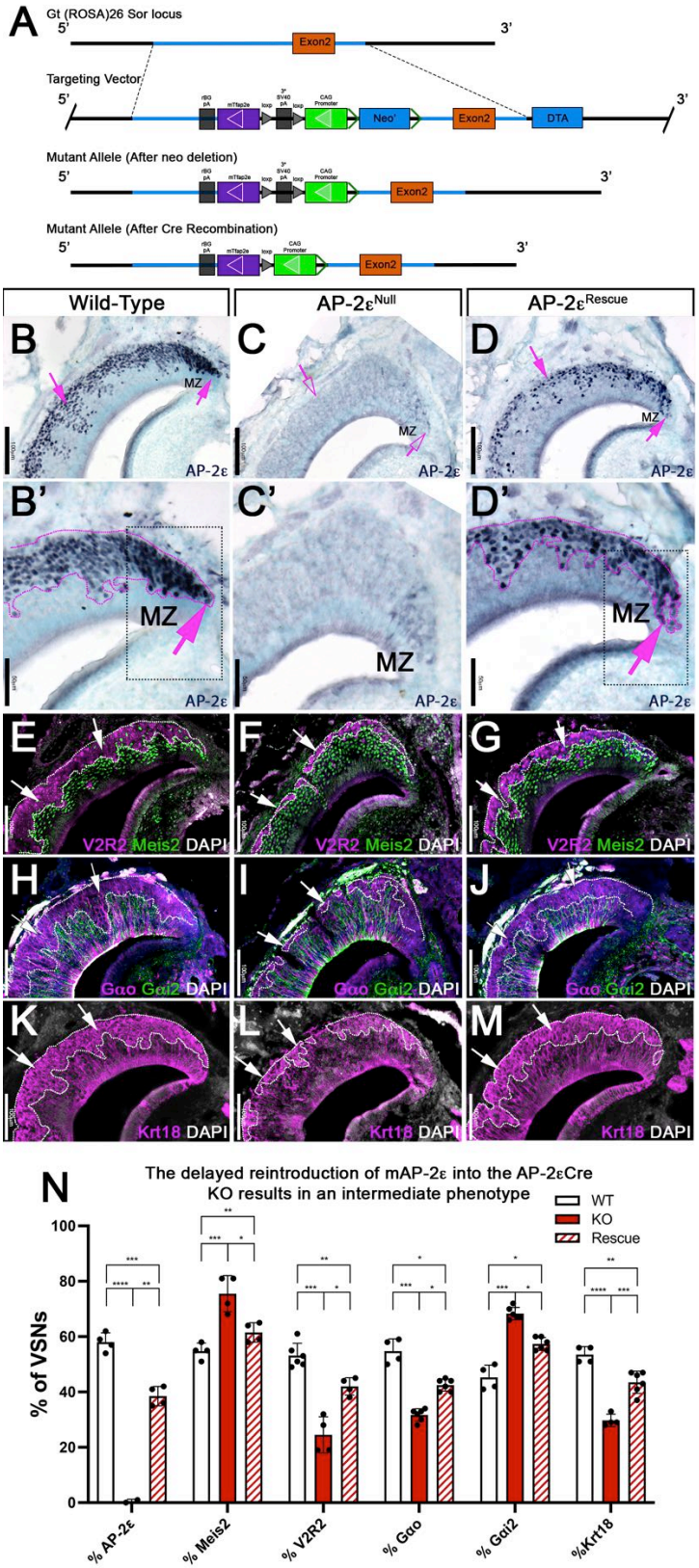

1332
1333

1334 **FIGURE 3**

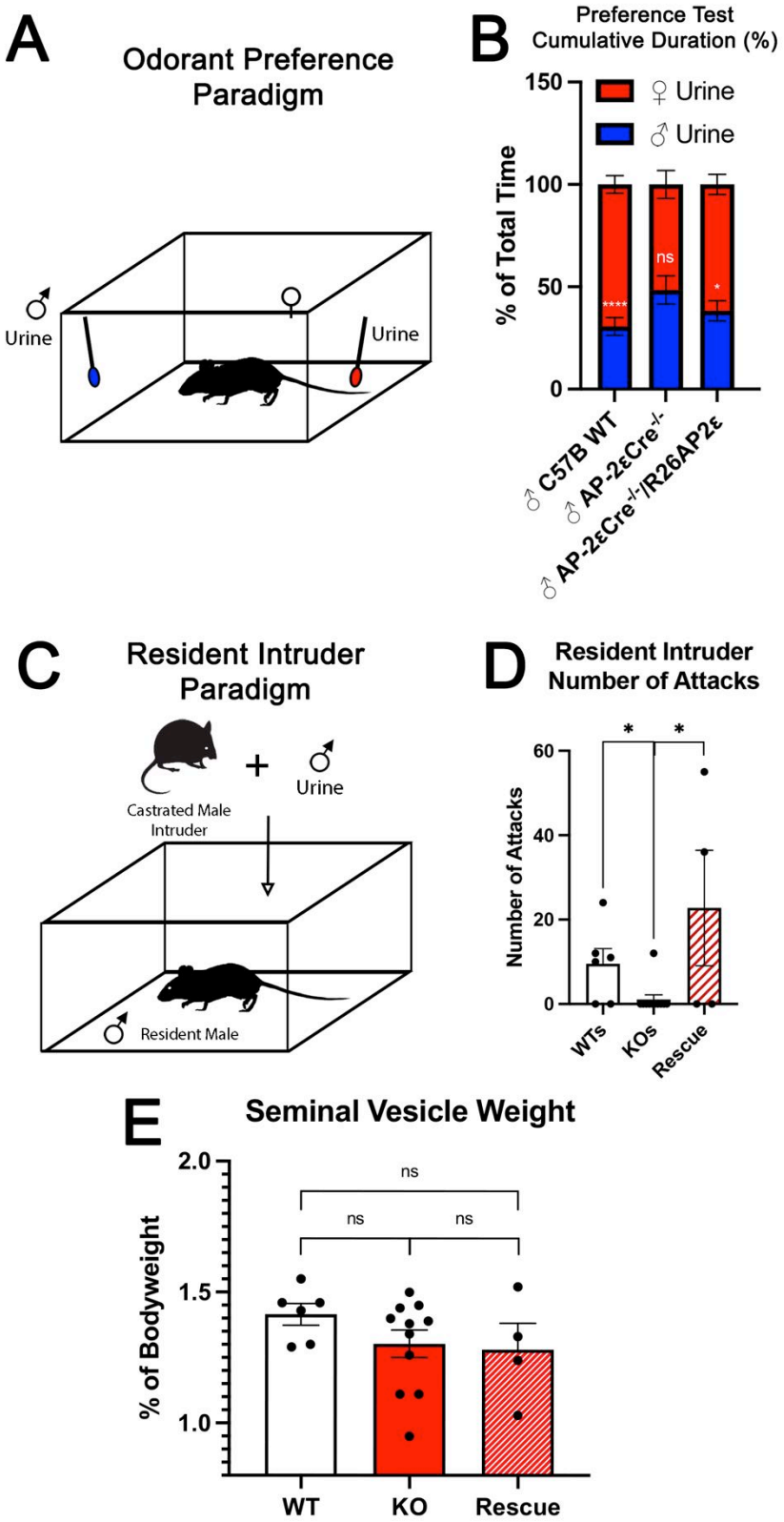

1335

FIGURE 4

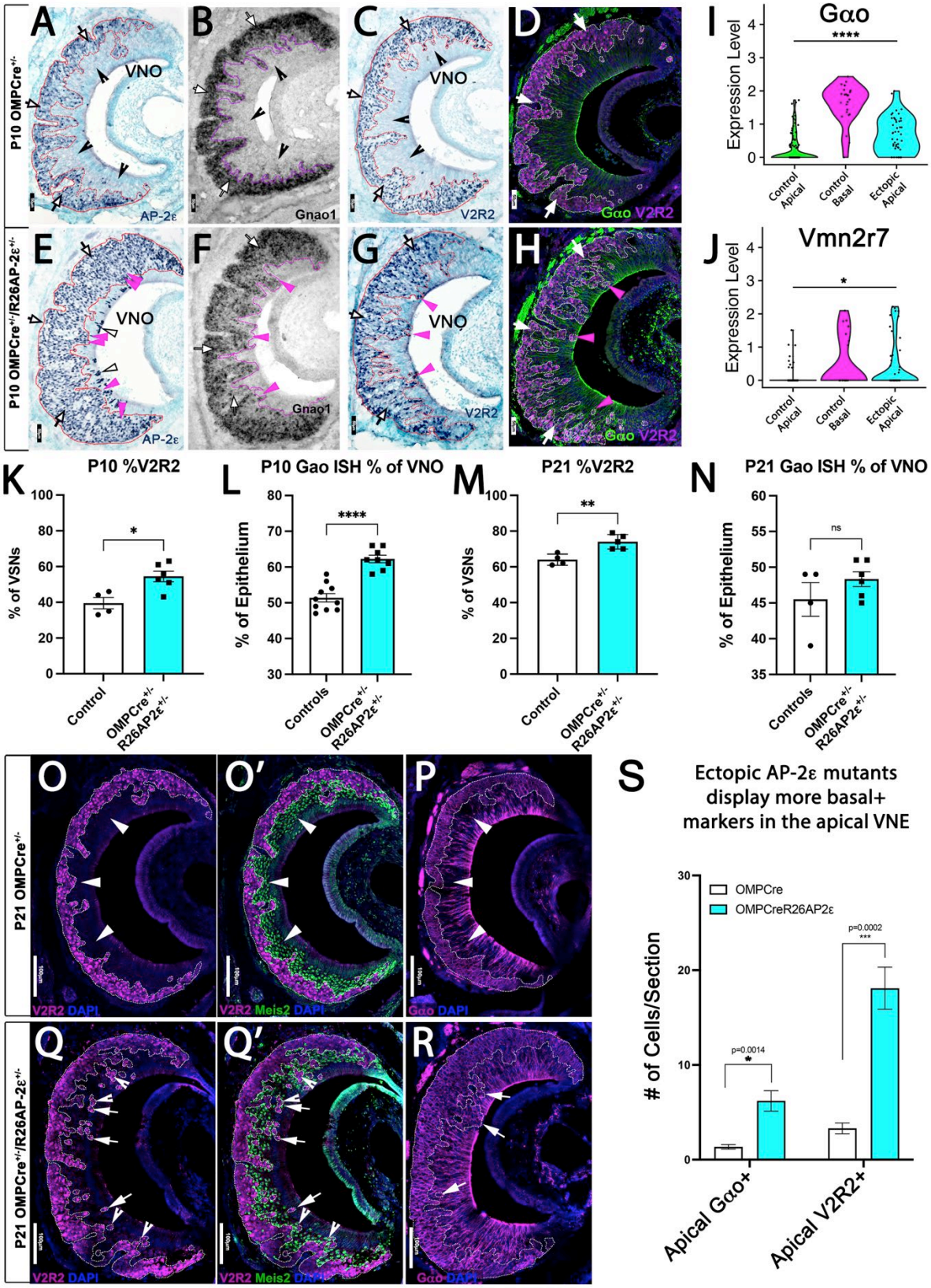
A
B
C
D
E
F
G
H
I
J
K
L
M
N
O
O′
P
Q
Q′
R
S
P10 OMPCre+/-
P10 OMPCre+/-/R26AP-2ε+/-
VNO
AP-2ε
Gnao1
V2R2
Gαo V2R2
Gαo
Vmn2r7
Expression Level
Control Apical
Control Basal
Ectopic Apical
P10 %V2R2
P10 Gao ISH % of VNO
P21 %V2R2
P21 Gao ISH % of VNO
% of VSNs
% of Epithelium
Control
Controls
OMPCre+/- R26AP2ε+/-
ns
P21 OMPCre+/-
P21 OMPCre+/-/R26AP-2ε+/-
V2R2 DAPI
V2R2 Meis2 DAPI
Gαo DAPI
Ectopic AP-2ε mutants display more basal+ markers in the apical VNE
OMPCre
OMPCreR26AP2ε
# of Cells/Section
p=0.0014
p=0.0002
Apical Gαo+
Apical V2R2+

FIGURE 5

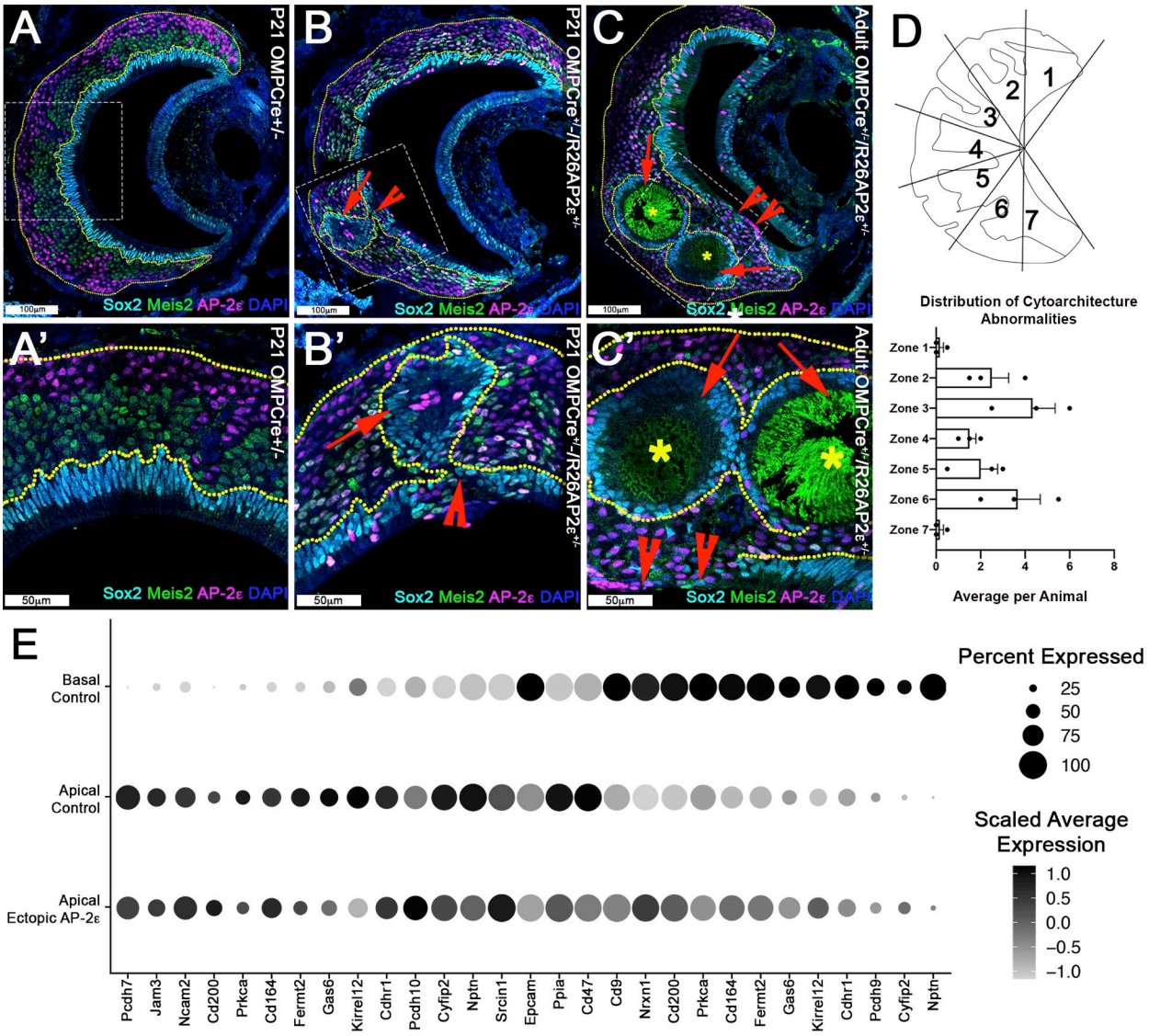
A
P21 OMPCre+/-
B
P21 OMPCre+/-/R26AP2ε+/-
C
Adult OMPCre+/-/R26AP2ε+/-
Sox2 Meis2 AP-2ε DAPI
100µm
A'
B'
C'
50µm
D
1
2
3
4
5
6
7
Distribution of Cytoarchitecture Abnormalities
Zone 1
Zone 2
Zone 3
Zone 4
Zone 5
Zone 6
Zone 7
0
2
4
6
8
Average per Animal
E
Basal Control
Apical Control
Apical Ectopic AP-2ε
Pcdh7
Jam3
Ncam2
Cd200
Prkca
Cd164
Fermt2
Gas6
Kirrel12
Cdhr1
Pcdh10
Cyfip2
Nptn
Srcin1
Epcam
Ppia
Cd47
Cd9
Nrxn1
Cd200
Prkca
Cd164
Fermt2
Gas6
Kirrel12
Cdhr1
Pcdh9
Cyfip2
Nptn
Percent Expressed
25
50
75
100
Scaled Average Expression
1.0
0.5
0.0
−0.5
−1.0

1348
1349 **FIGURE 6**

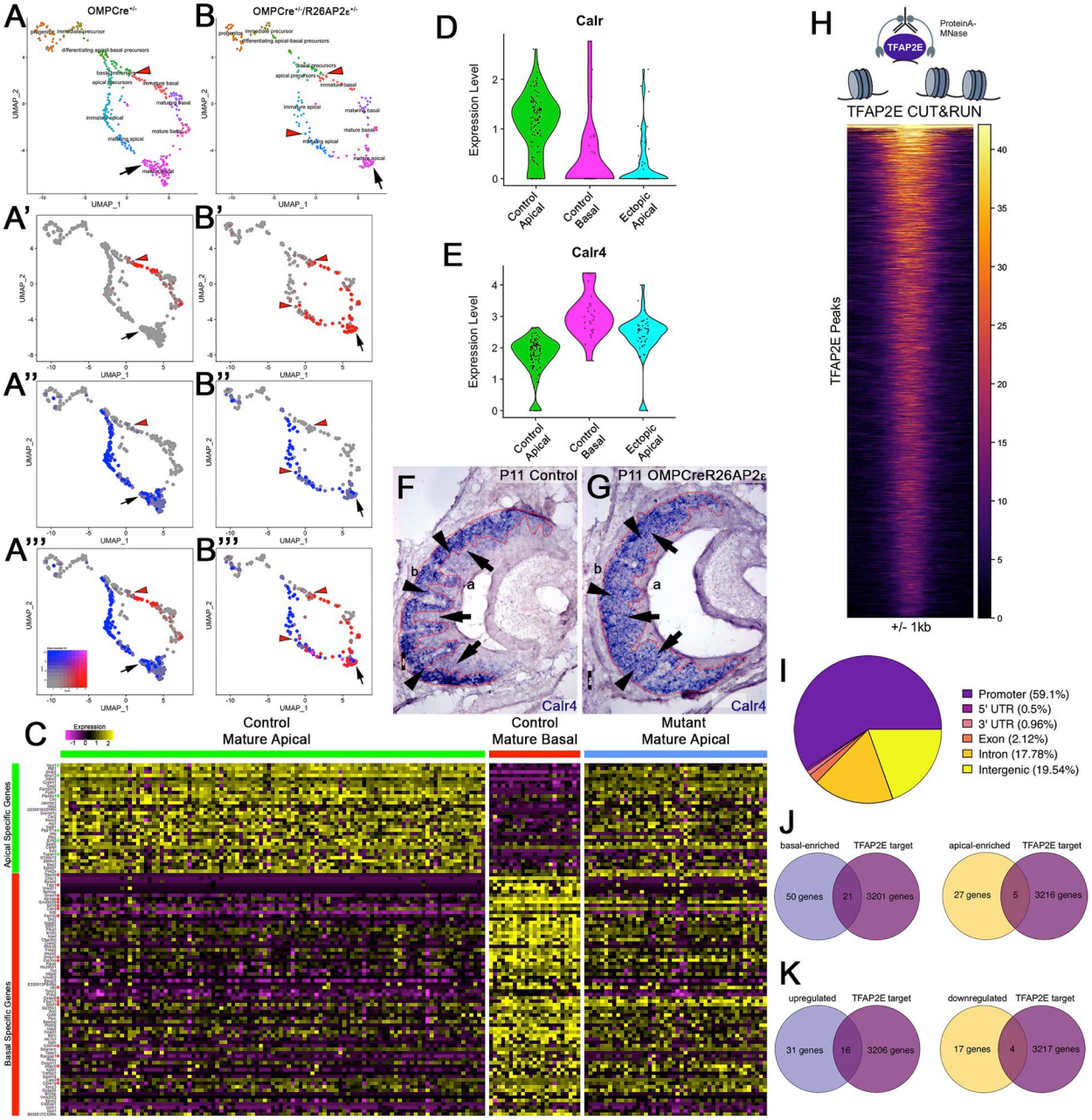

1350
1351
1352
1353
1354
1355

1356 **FIGURE 7**

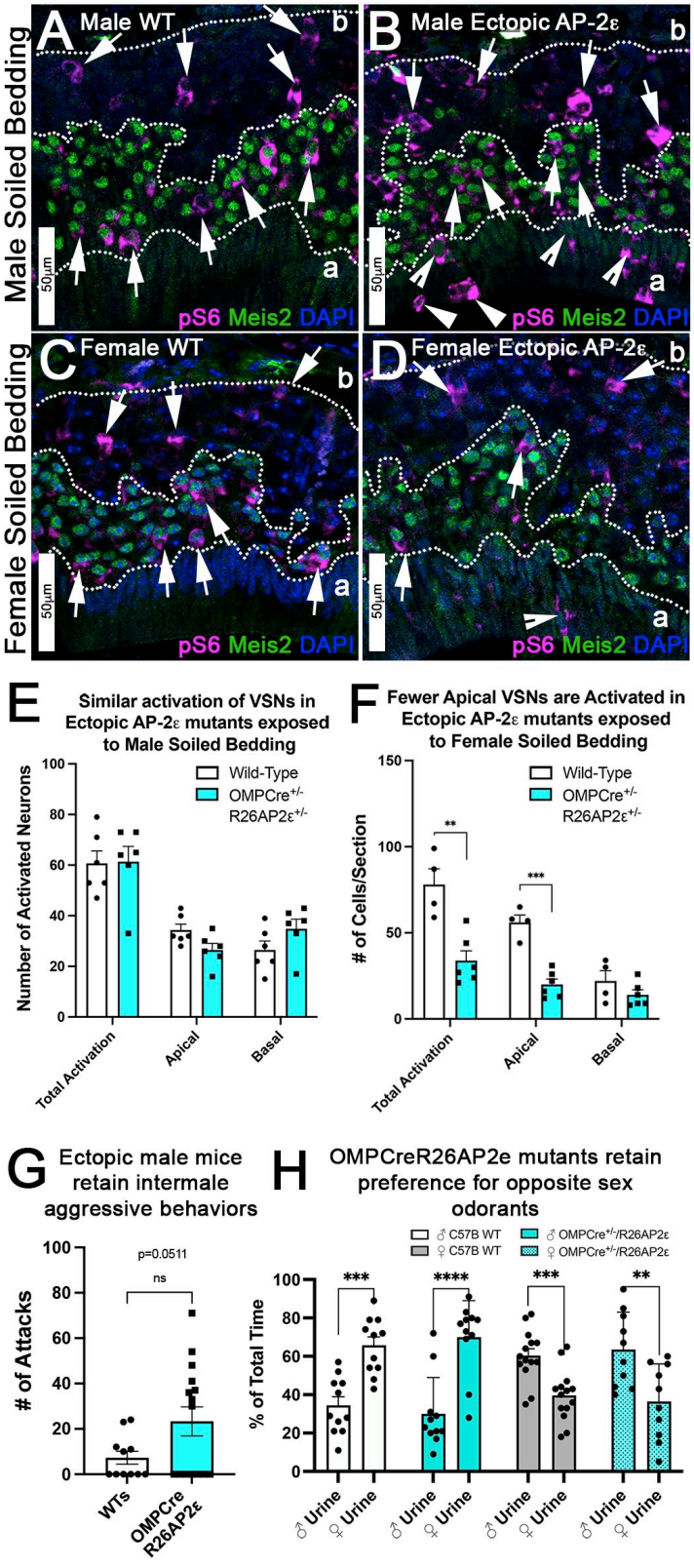

1357
1358

1359 **SUPPLEMENTARY FIGURES**

1360

1361

1362

1363 **FIGURE S1**

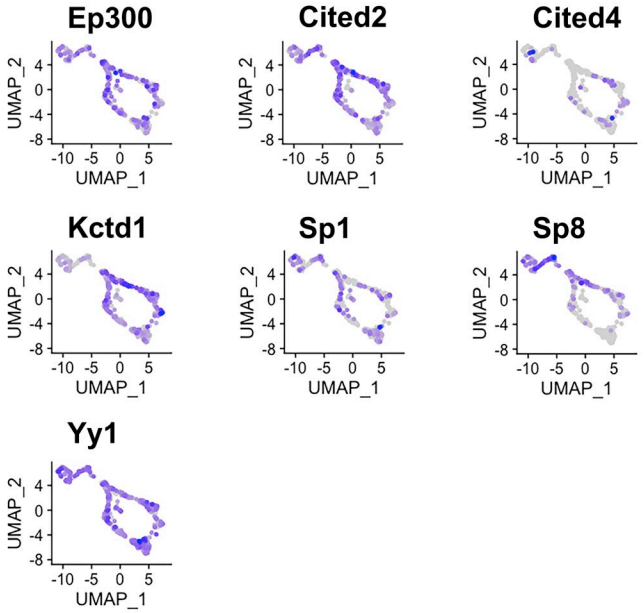

1364

1365

1366

1367

1368
1369 **FIGURE S2**

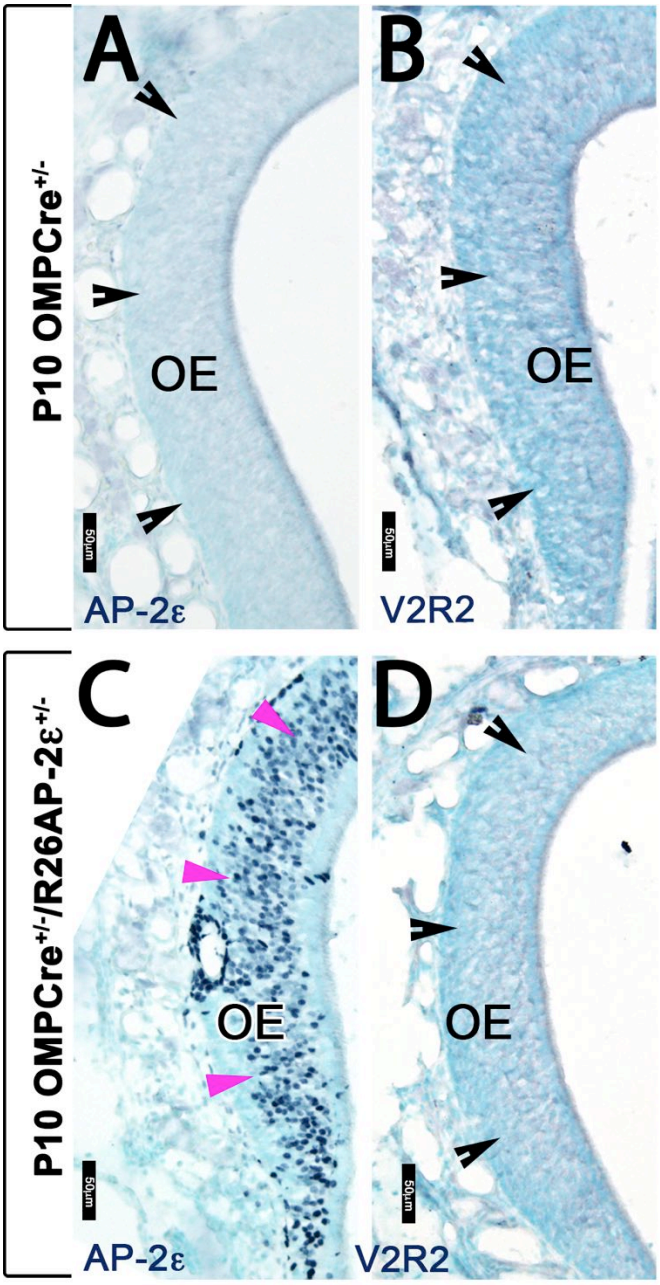

1370
1371
1372
1373
1374
1375
1376
1377
1378
1379
1380

FIGURE S3

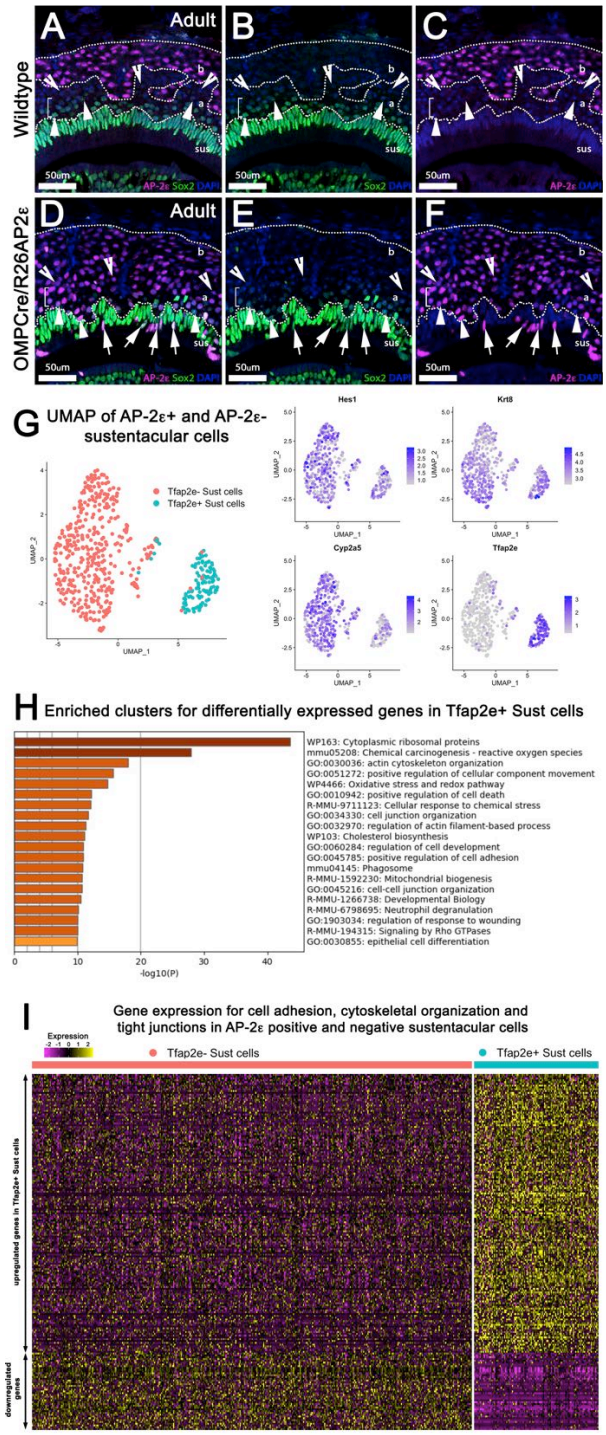
A
Adult
B
C
Wildtype
b
a
sus
50um
AP-2ε Sox2 DAPI
D
Adult
E
F
OMPCre/R26AP2ε
G
UMAP of AP-2ε+ and AP-2ε- sustentacular cells
Tfap2e- Sust cells
Tfap2e+ Sust cells
UMAP_1
UMAP_2
Hes1
Krt8
Cyp2a5
Tfap2e
H
Enriched clusters for differentially expressed genes in Tfap2e+ Sust cells
WP163: Cytoplasmic ribosomal proteins
mmu05208: Chemical carcinogenesis - reactive oxygen species
GO:0030036: actin cytoskeleton organization
GO:0051272: positive regulation of cellular component movement
WP4466: Oxidative stress and redox pathway
GO:0010942: positive regulation of cell death
R-MMU-9711123: Cellular response to chemical stress
GO:0034330: cell junction organization
GO:0032970: regulation of actin filament-based process
WP103: Cholesterol biosynthesis
GO:0060284: regulation of cell development
GO:0045785: positive regulation of cell adhesion
mmu04145: Phagosome
R-MMU-1592230: Mitochondrial biogenesis
GO:0045216: cell-cell junction organization
R-MMU-1266738: Developmental Biology
R-MMU-6798695: Neutrophil degranulation
GO:1903034: regulation of response to wounding
R-MMU-194315: Signaling by Rho GTPases
GO:0030855: epithelial cell differentiation
-log10(P)
I
Gene expression for cell adhesion, cytoskeletal organization and tight junctions in AP-2ε positive and negative sustentacular cells
Expression
Tfap2e- Sust cells
Tfap2e+ Sust cells
upregulated genes in Tfap2e+ Sust cells
downregulated genes

FIGURE S4

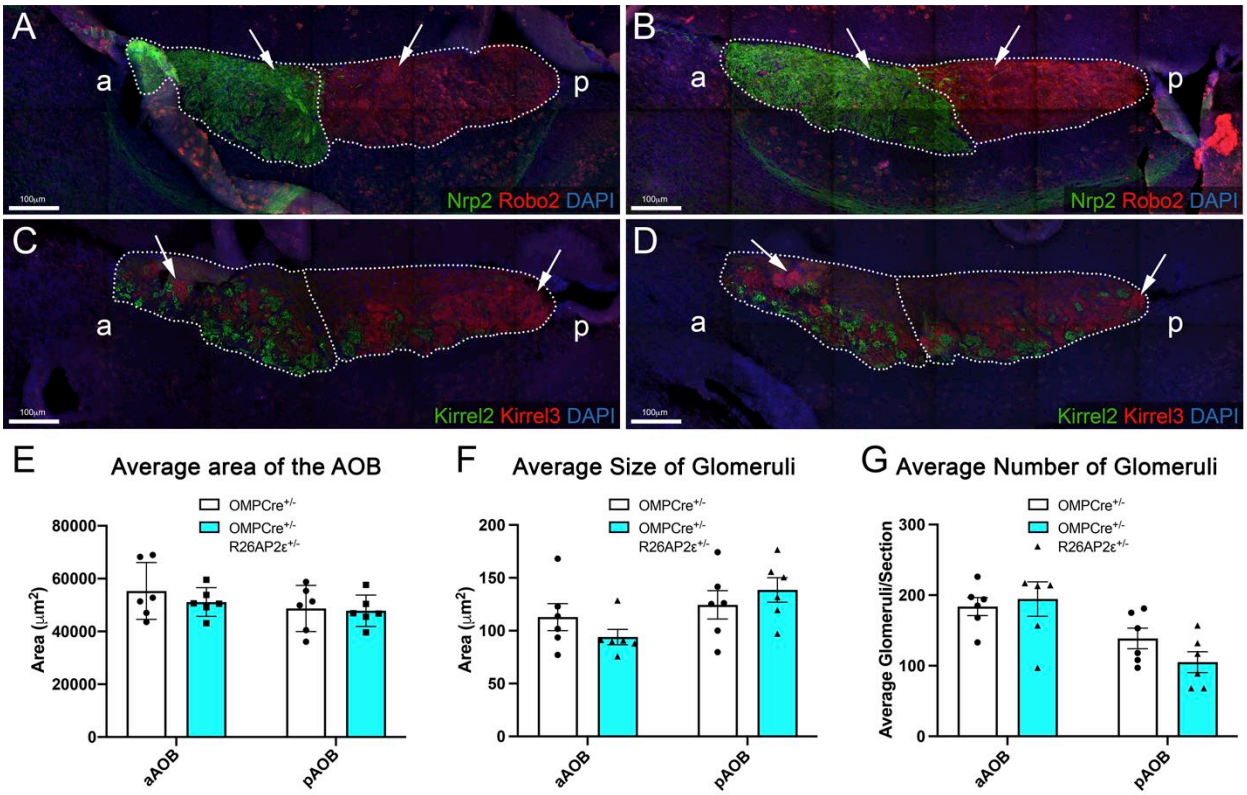
A
a
p
Nrp2 Robo2 DAPI
B
a
p
Nrp2 Robo2 DAPI
C
a
p
Kirrel2 Kirrel3 DAPI
D
a
p
Kirrel2 Kirrel3 DAPI
E
Average area of the AOB
OMPCre+/-
OMPCre+/- R26AP2ε+/-
Area (μm2)
80000
60000
40000
20000
0
aAOB
pAOB
F
Average Size of Glomeruli
OMPCre+/-
OMPCre+/- R26AP2ε+/-
Area (μm2)
200
150
100
50
0
aAOB
pAOB
G
Average Number of Glomeruli
OMPCre+/-
OMPCre+/- R26AP2ε+/-
Average Glomeruli/Section
300
200
100
0
aAOB
pAOB

1408 **FIGURE S5**

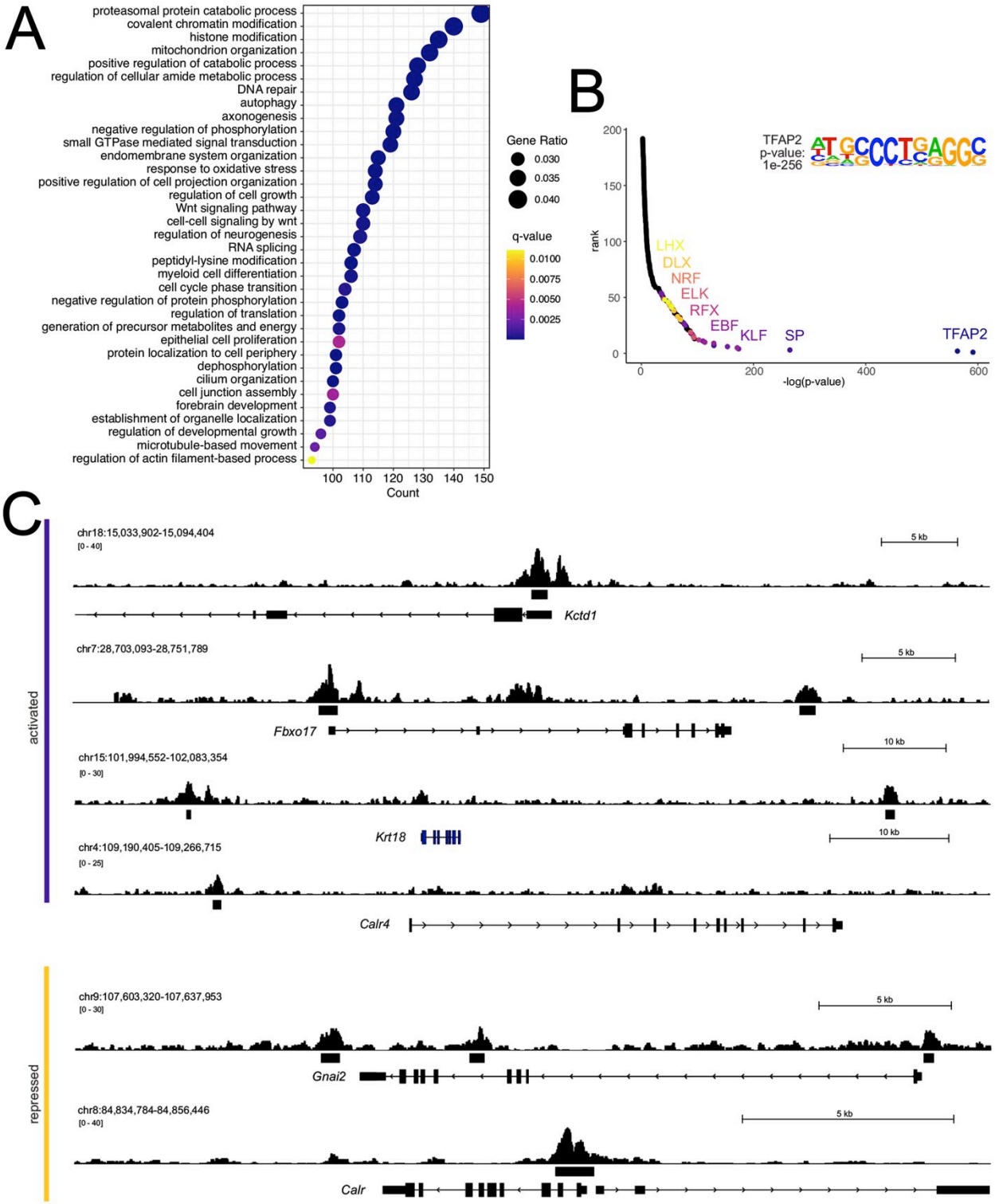

1409
1410
1411

1412 **FIGURE S6**

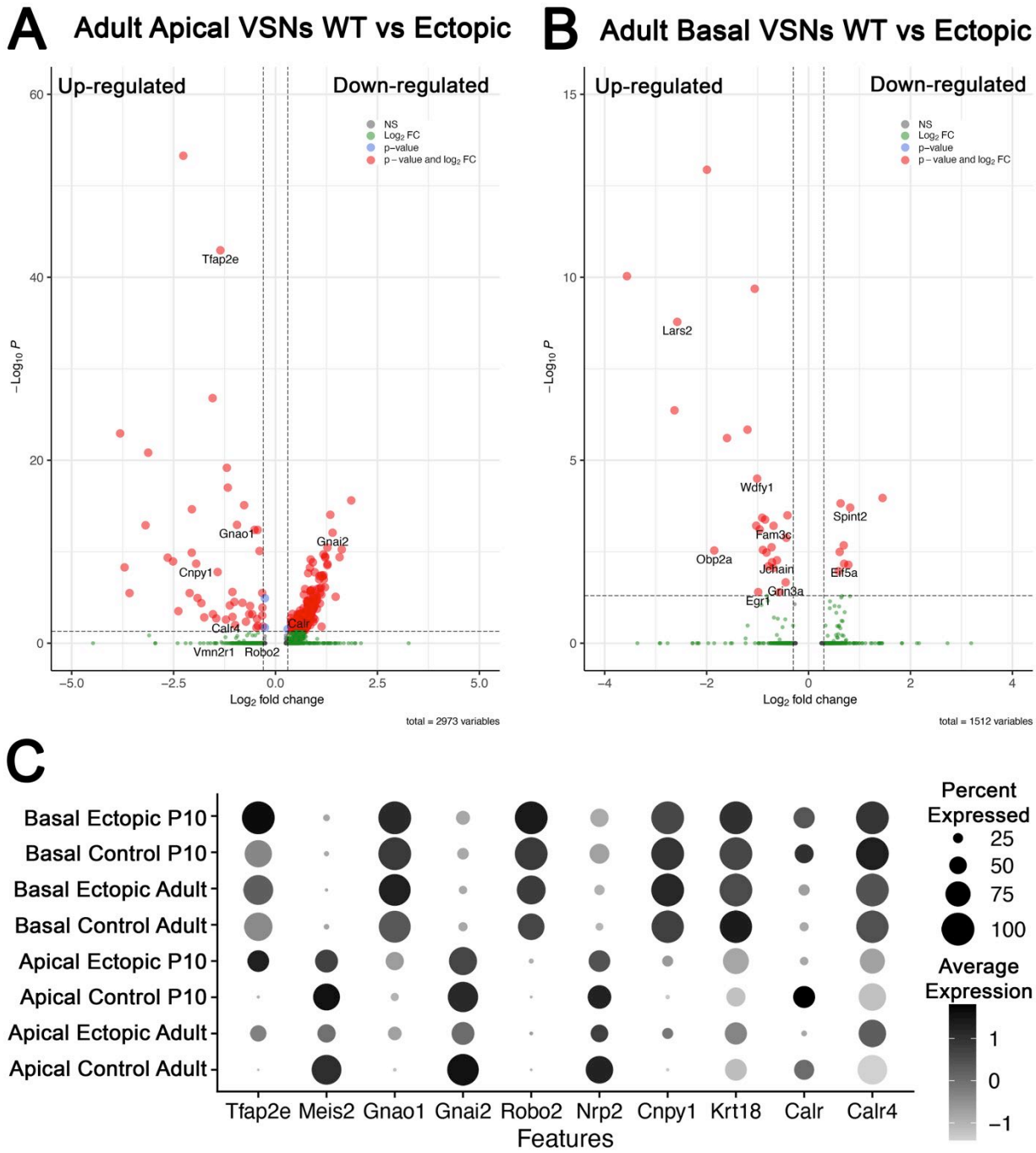

1413
1414
1415
1416
1417
1418
1419
1420
1421

Supplementary Table S1

Differentially expressed genes in mature apical and basal VSNs

Apically Enriched Genes					
Gene Name	P. Value	Average Log Fold Change	Mature Basal %	Mature Apical %	Adjusted P.Value
Nsg1	2.19E-13	-1.9461937	0.87	0.991	4.77E-09
Rtp1	3.99E-13	-1.7210806	0.13	0.972	8.69E-09
Gnai2	1.21E-12	-3.2758293	0.261	0.963	2.63E-08
Gng13	1.44E-12	-2.4998775	0.565	0.981	3.14E-08
Meis2	1.46E-12	-2.3994924	0.087	0.944	3.18E-08
Cystm1	2.60E-12	-1.1223905	0.913	1	5.66E-08
Gng2	4.70E-12	-1.8780287	0.696	0.963	1.02E-07
Fam241a	2.15E-11	-1.3441602	0.304	0.925	4.68E-07
Pcdh7	5.79E-11	-1.1606574	0.043	0.869	1.26E-06
Plekhb1	3.29E-10	-0.8073116	0.739	0.991	7.16E-06
Ckb	5.70E-10	-0.942904	0.957	1	1.24E-05
Jakmip1	2.13E-09	-0.7864416	0.13	0.841	4.65E-05
Nrp2	2.48E-09	-0.9997662	0.565	0.925	5.41E-05
G630016G05Rik	3.62E-09	-0.8518453	0	0.766	7.89E-05
Gramd1c	6.12E-09	-0.8132581	0.304	0.869	1.33E-04
Car2	1.29E-08	-0.871219	0.783	0.963	2.82E-04
Socs2	1.40E-08	-0.8762327	0.913	0.981	3.04E-04
Aig1	1.33E-07	-0.6442775	0.478	0.869	2.91E-03
Sgpl1	1.38E-07	-0.750675	0.652	0.953	3.01E-03
Ppp1r1a	1.62E-07	-0.6387545	0.87	0.953	3.53E-03
Nfix	1.63E-07	-0.6919687	0.087	0.71	3.55E-03
Rtp2	2.67E-07	-0.6124008	0.783	0.925	5.81E-03
Eml2	3.24E-07	-0.4522206	0	0.645	7.05E-03
Spef2	3.76E-07	-0.6257323	0.522	0.907	8.19E-03
Cartpt	6.02E-07	-0.504793	0.957	0.963	1.31E-02
Esd	6.05E-07	-0.5783619	0.174	0.748	1.32E-02
Tspan1	7.99E-07	-0.6642304	0.304	0.785	1.74E-02
S100a13	1.18E-06	-0.6578302	0.217	0.72	2.58E-02
Zdhhc3	1.22E-06	-0.6494611	0.609	0.879	2.65E-02
Bag1	1.60E-06	-0.4936463	0.87	0.972	3.48E-02
Exosc7	1.70E-06	-0.4935659	0.522	0.841	3.71E-02
Prxl2a	1.95E-06	-0.6048927	0.957	1	4.24E-02

Basally Enriched Genes					
Gene Name	P. Value	Average Log Fold Change	Mature Basal %	Mature Apical %	Adjusted P.Value
Tfap2e	2.71E-23	1.01282475	0.87	0.019	5.90E-19
Cnpy1	1.23E-22	2.05509001	1	0.093	2.69E-18
Robo2	3.77E-22	0.90330448	0.957	0.056	8.20E-18
Tafa1	4.72E-21	0.96728089	0.826	0.028	1.03E-16
Vmn2r1	2.11E-19	1.2793116	0.783	0.028	4.59E-15
Sphkap	6.49E-15	0.28031925	0.522	0	1.41E-10
Gnao1	6.12E-14	1.42314493	0.957	0.327	1.33E-09
Apmap	1.17E-13	1.58179511	1	0.916	2.55E-09
Gm36028	1.19E-13	2.53665489	1	0.682	2.58E-09
Krt18	2.60E-13	1.6051759	1	0.673	5.67E-09
Calr4	6.57E-13	1.39565197	1	0.916	1.43E-08
Krt8	1.51E-12	1.68676872	0.957	0.551	3.28E-08
Fam3c	1.65E-12	1.07729387	1	0.664	3.60E-08
Dio3	1.68E-12	0.40528977	0.478	0.009	3.65E-08
Agpat5	1.79E-12	1.08439932	1	0.514	3.89E-08
Sdf2l1	5.07E-12	1.50705224	1	0.879	1.10E-07
Pdia3	6.16E-12	0.86129121	1	1	1.34E-07
Itm2b	7.96E-12	1.18425959	1	1	1.73E-07
Manf	1.07E-11	1.37611844	1	0.953	2.33E-07
Cfap300	2.16E-11	0.77700954	0.957	0.421	4.71E-07
Creld2	2.17E-11	1.00229149	0.957	0.523	4.73E-07
Shisa8	2.58E-11	0.36615576	0.391	0	5.63E-07
Fkbp2	2.90E-11	0.72341813	1	0.907	6.32E-07
Hspa5	5.22E-11	1.40010137	1	0.981	1.14E-06
Dnajc3	6.37E-11	1.1592286	0.957	0.729	1.39E-06
Dio3os	7.37E-11	0.49488572	0.565	0.047	1.60E-06
Pdia6	1.07E-10	1.14235131	1	0.888	2.32E-06
Hsp90b1	2.05E-10	0.85553036	1	0.991	4.47E-06
Dut	2.84E-10	0.76430257	1	0.86	6.19E-06
Mfge8	3.07E-10	1.07748862	0.957	0.794	6.68E-06
Vmn2r2	4.22E-10	1.35916407	0.391	0.009	9.19E-06
Dpysl3	1.30E-09	1.17193306	0.957	0.757	2.84E-05
E330013P04Rik	1.41E-09	0.35778211	0.609	0.084	3.08E-05
Mt3	1.88E-09	0.57279227	0.739	0.215	4.09E-05
Tubb3	3.51E-09	0.64687805	1	0.963	7.64E-05
Prdx2	3.78E-09	0.72277812	1	0.953	8.23E-05

Osbpl9	5.01E-09	0.83250073	0.913	0.813	1.09E-04
Fbxo17	5.56E-09	0.50343797	0.652	0.15	1.21E-04
Stbd1	6.55E-09	1.09297275	1	0.963	1.43E-04
Slc35b1	9.68E-09	0.68626655	0.957	0.738	2.11E-04
Rd3	1.35E-08	0.5858953	1	0.972	2.93E-04
Gchfr	1.35E-08	0.32772543	0.522	0.065	2.94E-04
Ppib	1.55E-08	0.6188014	1	0.972	3.38E-04
Selenof	1.55E-08	0.51120029	1	0.981	3.38E-04
Plxdc2	1.59E-08	0.2695123	0.435	0.037	3.45E-04
Ugp2	1.63E-08	0.90939627	0.957	0.794	3.56E-04
Tmed3	2.62E-08	0.50570554	1	0.916	5.71E-04
B2m	3.78E-08	1.26181829	0.913	0.542	8.23E-04
Akr1b3	6.06E-08	0.97983293	0.87	0.523	1.32E-03
Optn	7.24E-08	0.31830823	0.478	0.065	1.58E-03
Golim4	8.68E-08	0.52488666	0.913	0.551	1.89E-03
Selenom	1.04E-07	0.49334844	1	1	2.26E-03
Tppp3	1.17E-07	0.89025439	0.652	0.168	2.55E-03
Racgap1	1.58E-07	0.61403494	0.913	0.561	3.45E-03
Rhou	1.72E-07	0.39239137	0.609	0.15	3.74E-03
Dnajb11	1.76E-07	0.70097289	0.957	0.944	3.84E-03
Mfap3l	2.28E-07	0.28167932	0.565	0.103	4.96E-03
Kctd1	2.38E-07	0.88812556	0.913	0.542	5.17E-03
Traf3ip3	3.03E-07	0.73231367	0.391	0.037	6.61E-03
Galnt18	3.24E-07	0.55665364	0.826	0.411	7.05E-03
Calb2	3.73E-07	0.43308595	1	1	8.13E-03
Cdkn1a	3.82E-07	0.5373044	0.957	0.907	8.33E-03
Spcs3	4.63E-07	0.55754661	0.957	0.832	1.01E-02
Dusp26	4.98E-07	0.54873277	0.957	0.822	1.08E-02
Bri3bp	6.03E-07	0.36483009	0.522	0.112	1.31E-02
Vmn2r53	1.01E-06	2.68138046	0.217	0	2.21E-02
Spcs2	1.09E-06	0.59703272	0.957	0.944	2.37E-02
Carhsp1	1.32E-06	0.38531423	0.522	0.112	2.87E-02
Dclk1	2.00E-06	0.39895571	0.826	0.327	4.35E-02
Guk1	2.05E-06	0.5985497	0.913	0.897	4.45E-02
B230217C12Rik	2.24E-06	0.424191	1	0.813	4.87E-02

Supplementary Table S2

Significantly Up and Down Regulated Genes when Tfap2e/AP-2ε is ectopically expressed

Significantly Down-Regulated Genes

Gene Name	P. Value	Average Log Fold Change	Mature Basal %	Mature Apical %	Adjusted P.Value
Nsg1	1.05E-19	-1.026049429	0.978	0.991	2.28E-15
Ckb	3.16E-13	-0.832807392	0.957	1	6.89E-09
Plekhb1	1.02E-12	-0.66365877	0.804	0.991	2.23E-08
Calr	1.99E-12	-0.848017913	0.326	0.879	4.33E-08
Gng13	3.92E-11	-0.851799068	0.978	0.981	8.55E-07
Prdx1	6.92E-11	-0.670948424	0.674	0.925	1.51E-06
Ftl1-ps1	5.23E-10	-1.01755918	0.5	0.822	1.14E-05
Calm2	7.50E-09	-0.359436172	1	1	1.63E-04
Rps4x	9.27E-09	-0.462870937	0.978	1	2.02E-04
Chgb	5.21E-08	-0.509353353	0.63	0.907	1.13E-03
Obp2a	5.51E-08	-0.803452485	0.5	0.832	1.20E-03
Esd	1.16E-07	-0.447142323	0.391	0.748	2.54E-03
Eml2	1.21E-07	-0.290177152	0.152	0.645	2.63E-03
Lcn3	3.31E-07	-0.704072872	0.413	0.804	7.22E-03
Nqo1	4.44E-07	-1.080448365	0.239	0.636	9.68E-03
Ppp1r1a	6.98E-07	-0.395511356	0.935	0.953	1.52E-02
Id4	9.43E-07	-0.48810942	0.283	0.673	2.05E-02
Tspan1	1.12E-06	-0.469458509	0.543	0.785	2.45E-02
Cpe	1.20E-06	-0.310695303	1	1	2.61E-02
Gt(ROSA)26Sor	1.32E-06	-0.45231242	0.717	0.832	2.88E-02
Tstd1	1.35E-06	-0.387425488	0.935	0.963	2.94E-02

Significantly Up-Regulated Genes

Gene Name	P. Value	Average Log Fold Change	Mature Basal %	Mature Apical %	Adjusted P.Value
Abca7	2.79E-10	0.467733988	0.848	0.393	6.07E-06
Apmap	4.12E-08	0.499754357	1	0.916	0.000898417
Calb2	2.04E-08	0.32207374	1	1	0.00044526
Calr4	6.89E-11	0.580533012	0.935	0.916	1.50177E-06
Ccdc136	1.17E-08	0.433981247	0.696	0.252	0.000254306
Cdkn1a	2.88E-07	0.455507857	1	0.907	0.006262153
Cst6	3.50E-14	1.099290617	0.935	0.794	7.62225E-10
Dbi	3.62E-12	1.062519896	0.957	0.813	7.8747E-08
Dio3os	1.34E-15	0.383916442	0.652	0.047	2.92422E-11

Dlx4	8.01E-09	0.438918572	0.783	0.327	0.000174394
Dnajc3	5.15E-07	0.423663136	0.913	0.729	0.011213757
Dusp15	1.60E-08	0.288331862	0.587	0.14	0.00034899
Dync1i1	3.35E-08	0.495088228	0.848	0.533	0.000729768
Enpp1	1.92E-06	0.36206672	0.891	0.551	0.041912856
Fam3c	3.92E-07	0.381794339	0.913	0.664	0.008538247
Fbxo17	1.06E-17	0.668034836	0.804	0.15	2.31481E-13
Fmnl2	1.47E-06	0.294102212	0.717	0.346	0.031962548
Gm36028	1.51E-15	1.565013376	0.935	0.682	3.27889E-11
Gnao1	5.65E-07	0.344705173	0.783	0.327	0.012315414
Golim4	1.06E-06	0.393270819	0.804	0.551	0.023038974
Itpr1	1.54E-12	0.42801754	0.696	0.131	3.35489E-08
Jak1	1.57E-07	0.423690646	0.978	0.972	0.003418952
Kctd1	7.64E-16	0.85428255	0.978	0.542	1.66452E-11
Kctd17	5.75E-08	0.383015359	0.957	0.907	0.001251818
Khdrbs1	9.29E-07	0.388803088	0.935	0.692	0.020230178
Krt18	2.14E-06	0.448568282	0.935	0.673	0.046678066
Lrrc58	5.13E-09	0.336180339	0.717	0.243	0.00011176
Mab21l2	3.38E-11	0.342240813	0.37	0	7.3587E-07
Mapk8ip2	1.52E-07	0.38275929	1	0.963	0.003310007
Mfap3l	5.77E-11	0.330339336	0.609	0.103	1.25577E-06
Mfge8	7.50E-08	0.517438515	0.913	0.794	0.001634157
Mgat5	3.40E-07	0.328523537	0.87	0.486	0.007398101
Mt3	2.31E-12	0.486337274	0.761	0.215	5.03186E-08
Osbpl9	3.00E-09	0.615805448	0.957	0.813	6.544E-05
Pir	6.37E-09	0.572417884	0.848	0.486	0.000138796
Ptprd	4.71E-07	0.333394508	0.522	0.14	0.010266165
Racgap1	1.11E-06	0.405891754	0.87	0.561	0.024189968
Rims3	2.59E-07	0.430808566	1	0.916	0.005638623
Rmdn3	2.84E-08	0.443857099	0.783	0.458	0.000618452
Rpl11	2.14E-07	0.287691748	0.978	0.981	0.004668027
Smchd1	6.17E-13	1.30491047	0.935	0.598	1.34339E-08
Spats2	3.38E-12	0.613696552	0.957	0.832	7.36795E-08
Stbd1	1.62E-08	0.724116114	0.978	0.963	0.000353362
Suox	9.51E-08	0.433632116	0.739	0.364	0.002071784
Tafa1	1.26E-13	0.39251169	0.522	0.028	2.74227E-09
Tfap2e	7.33E-30	2.020231614	0.935	0.019	1.597E-25
Tsnax	2.00E-08	0.574771495	1	1	0.000435139